TOPSAFE

Dubrovnik, Croatia, 30.09 - 3.10.2008

TopSafe 2008

Transactions

Dubrovnik, Croatia
30.9. - 3.10.2008

HND

AEN NEA

IAEA International Atomic Energy Agency
Atoms For Peace

European Nuclear Society
Rue Belliard 65
1040 Brussels, Belgium
Phone + 32 2 505 30 54
Fax +32 2 502 39 02
E-mail ens@euronuclear.org
Internet www.euronuclear.org

ISBN 978-92-95064-06-5

These transactions contain all contributions submitted by 30 September 2008.

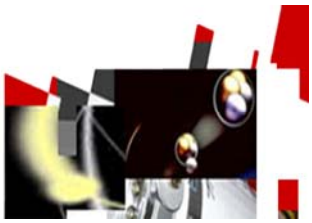

Research Reactors

THE BORAX ACCIDENT IN THE JHR*

(Jules Horowitz Reactor)*

B.Maugard, JP.Elie, P.Trémodeux, F.Witters, P.Sireta, Ch.Döderlein, J.Di Salvo, C.Brayer, D.Tarabelli, Y.Margerit, F.Jourdain, G.Ducros, S.Maillard
CEA/DEN(1)
Centre d'Etudes Nucléaires de Cadarache
13108 StPaul lez Durance
bruno.maugard@cea.fr, jean-philippe.elie@cea.fr, pascal.tremodeux@cea.fr, frederic.witters@cea.fr, patricia.sireta@cea.fr, christoph.doderlein@cea.fr, jacques.disalvo@cea.fr, claude.brayer@cea.fr, didier.tarabelli@cea.fr, yves.margerit@cea.fr, franck.jourdain@cea.fr, gerard.ducros@cea.fr, serge.maillard@cea.fr

D.Iracane, P.Lemoine, O.Grégoire, S.Kokh, M.Martin, P.Salvatore, E.Richebois, E.Royer, Ph.Roblin, C.Van Wambeke, J.Segré, V.Faucher, P.Galon-Bruère
CEA/DEN(1)
Centre d'Etudes Nucléaires de Saclay
91191 Gif sur Yvette
daniel.iracane@cea.fr, patrick-marie.lemoine@cea.fr, olivier.gregoire@cea.fr, samuel.kokh@cea.fr, mathieu.martin@cea.fr, patricia.salvatore@cea.fr, edwige.richebois@cea.fr, eric.royer@cea.fr, philippe.roblin@cea.fr, christian.van-wambeke@cea.fr, jacques.segre@cea.fr, vincent.faucher@cea.fr, pascal.galon@cea.fr

G.Ratel, G.Berthoud
CEA/DEN(1)
Centre d'Etudes Nucléaires de Grenoble
38054 Grenoble
gilles.ratel@cea.fr, georges.berthoud@cea.fr

(1) Commissariat à l'Energie Atomique (CEA) – Direction de l'Energie Nucléaire (DEN)

ABSTRACT

The BORAX accident (Boiling Water Reactor Experiment) is the Mastered Severe Accident reference to be taken into account by the containment design of JHR. Two major stakes are concerned: the radiological consequences with respect to released activities and the mechanical consequences with verification of acceptable behaviour for the pool system. A reasonably conservative approach was developed in 2007-2008 to simulate the global phenomenon of this accident. A "BORAX calculation scheme" based on existing codes and specifically adapted or developed for the JHR application, was set up and will provide quantitative results.

1 INTRODUCTION

Beyond the four classical safety categories, the French safety methodology defines several situations integrating the Mastered Severe Accident (MSA) for which it is necessary to demonstrate that the consequences are controlled.

The BORAX accident (Boiling Water Reactor Experiment) is the MSA reference to be taken into account by the containment design of JHR [1]. Two major stakes are concerned: the radiological consequences with respect to released activities and the mechanical consequences with verification of acceptable behaviour for the pool system.

This conventional accident consists in a fast ejection of a control rod, leading to a nuclear power excursion and the fusion of a part of the nuclear fuel (actually aluminium alloy only). This is supposed to lead to a steam explosion generated by the violent interaction between liquid aluminium and the cooling water. This phenomenon consists of a complex and fast sequence of physical-chemical processes with different time and space scales.

This accident has been treated in the past for all French research reactors on the basis of a hypothetical thermal energy deposition close to 135 MJ and a mechanical efficiency of 9%. Consensual values for radionuclide transfer coefficients were chosen for the design phase of the reactor. Afterwards, experimental validations were performed, with real explosions on low scale mock ups to verify the safe behaviour of the second safety barrier.

The methodology proposed at the end of 2005 in the Preliminary Safety Report of the JHR consists in a more realistic approach. A thermal-dynamical approach of the accident scenario was particularly expected to improve our understanding of phenomenon.

A multi-disciplinary workshop was set up in mid-2007 with the goal of identifying and modelling the different phenomena involved in the Borax sequence. It led to the setting-up of a BORAX calculation scheme, enabling to quantify the different stages of the accident.

A reasonably conservative approach was thus developed in 2007-2008, based on existing codes and specifically adapted or developed for the JHR application. Code chaining or coupling are set up where necessary. A detailed assessment on accidents and experiments has been consecutively performed on research reactors in the world since the beginning of the nuclear era.

The accident has thus been chronologically divided into a few stages with characteristic durations varying from 1 to some 100 ms. For each stage, conservative hypothesises have been made in order to reasonably aggravate the consequences, related to the stakes.

2 THE INITIATING EVENT AND POWER TRANSIENT

The hypothetical failure of a control rod leads to a fast ejection of the absorber and a reactivity injection of about 3 $ in 0.1 second. Then the nuclear power rises and decreases very quickly by Doppler and void effect, leading to a thermal energy deposit in the fuel meat and the fuel cladding in a few hundredths of a second. A molten fuel crucible ($T>T_{f,Al}$) appears inside the plate, expanding and projecting a spray of fuel particles under pressure into the water volume close to the plates. One can imagine the extremely quick cascading propagation to neighbouring plates in the hotter area of the core.

The physics of this phase simultaneously combines neutron physics and thermal-hydraulics, and justifies the development of a 3D kinetics calculation scheme with coupling between CRONOS2 [2] and FLICA4 [3] codes, based on a simplification of the HORUS3D scheme [4,5].

The 3D neutronics simulation is performed with the CRONOS2 code, in an approach homogeneous on assembly level. The 6 group cross sections libraries, elaborated by the APOLLO2 code [6], have been parameterized for a fresh core, in fuel temperature, void ratio and absorber rod insertion level.

The assembly neutronics parameters are homogenised over the whole core for the resolution of the kinetics equations.

The coupled resolution of the coolant thermal-hydraulics and the fuel thermal problem is accomplished with the FLICA4 code. It's based on the modelling of the HORUS3D calculation scheme with the following modifications:

- adaptation of the thermal exchange and post dry-out vaporisation models,
- nucleate boiling is not taken into account,
- the fusion of aluminium taken into account in the modelling of the fuel materials physical properties,
- modelling of hydrogen production by radiolysis.

The fuel thermal modelling is based on the hypothesis that the U_3Si_2-Al meat fusion is limited to the simple fusion of the aluminium matrix: the U_3Si_2 particles dispersed within this aluminium matrix stay at solid state. We model the physical properties of the fissile meat by a homogenisation of the properties of the Uranium Silicide dispersed phase and the Al matrix.

The data exchange between CRONOS2 and FLICA4 is performed by the ISAS [7] coupling code.

The fast dilatation of the fuel plate, leading to a decrease of the size of the gap between the plates and to a negative reactivity feedback due to the under-moderation, is not considered in the model. The calculations are thus penalizing. This dilatation effect is probably significant and would minimize significantly the transient consequences.

FLICA4 and DULCINEE [8] codes are also separately used for 0D-kinetics sensitivity studies. The legitimacy of the use of 0D-kinetics model is based on the small size of the JHR core and the small deformation of the power distribution during the reactivity accident.

The objective of the CRONOS2-FLICA4 calculations is to obtain a realistic molten fuel ratio and the associated fusion kinetics, as well as the quantity of thermal energy deposited in the fuel, potentially transferable into the coolant.

The choice of the "end of accident" criteria is an important parameter of the setting up of the calculation scheme, as the geometrical variations of the fuel and its rapid loss of integrity are not being considered in the modelling.

3 FUEL - WATER INTERACTION

The MC3D code [9] simulates this key-phase with the injection of the molten fuel particles into the interaction volume and explicitly reproduces the thermal exchange between the fuel particles and water in a time of less than 30 ms. The water pressure rises in a rather isochoric manner up to some hundred bar within less than 1 ms. Then the water volume begins to warm up, decreasing its pressure at the same time. The relaxation of the vapour bubble pressure leads to a violent expansion of the bubble (steam explosion) and to an impulse of some ten bar, acting for several ms on the wall of the nuclear unit's pool.

The MC3D code is adapted for simulating this steam explosion phase and, in a second time, for calculating the impulse on the pool wall and ground after numerous rebounds and interferences.

Considering the rapidity of the phenomenon, the heat exchange by conduction is quiet insignificant and the fuel meat fusion leads to a mechanical strain on the clad with an increase of internal pressure.

We took the hypothesis of an instantaneous fragmentation of the molten aluminium drops, down to a final diameter close to 40 µm (BORAX specific injection mode). These aluminium drops originate from the clad and the aluminium matrix of the fuel meat. The U_3Si_2 particles, swept along in the spray of the molten aluminium, are supposed to stay at solid state and keep their 60 µm diameter.

The aluminium droplets and the U3Si2 grains have thus different diameters and temperatures and the MC3D code has been modified to describe the two populations of fragments.

Two injection scenarios are considered on the base of the coupled neutronics/thermalhydraulics calculations, which give the fuel melting kinetics: the first one assumes that the fuel particles are injected as soon as the fusion begins. The second supposes an instantaneous injection of the fuel into the water at the end of the fuel meat fusion, thus simulating a quick increase of the internal pressure in the meat until a violent failure of the clad.

In addition to the thermal energy of the molten fuel, the supplementary energy of the interaction of water with NaK, contained in irradiation devices, and the oxidation of aluminum is taken into account simultaneously and in a conservative manner, by increasing the mass of molten fuel at constant temperature.

Two types of calculation are considered:

- "Vessel" calculations, modelling the pressure vessel and the primary circuit piping with an adapted meshing; the points of interest are the pressure strains on the structures and the presence of water steam.
- "Pool" calculations with the hypothesis of an unrestricted steam explosion.

The first mentioned MC3D calculations, more representative, make possible the analysis of the vessel's failure mode and, in particular, the resistance of the vessel closure head (cannonball effect). They enable furthermore to estimate a potential amplification of the effect, due to the "confinement" during the short phase of the pressure rise.

The second type of calculations leads to a reasonably conservative assessment of the mechanical effects on the walls of the water block, a potential ejection of debris and the kinetics of the steam and incondensable gas bubble.

4 THE EVOLUTION OF THE VAPOUR AND INCONDENSABLE GAS BUBBLE

Immediately after the fuel and water interaction, the brutal expansion of the hot water drop leads to the formation of a bubble containing a mixture of steam and incondensable gas (fission gas, H_2 formed by aluminium oxydation and NaK- water reactions).

Several risks are considered :

- The formation of a water spray at the pool surface, with a potential impact on the containment, with entrainment of fuel debris into the containment hall, thus contributing to the dispersal of radioactive products and accelerating the pressure rise within the containment by direct heating,
- The ascension of bubbles to the surface, directly transporting fuel aerosols to the containment hall, in an analogous manner to phenomenon mentioned before but with microscopic particles.
- The amplification of the radiological consequences outside of the containment, because of a higher instantaneous source term and an accelerated pressure rise.

The structures inside the reactor pool do certainly contribute significantly to the fragmentation of important bubble, but this assumption is neglected in a conservative manner. Likewise, the presence of a considerable height of water above the core (9 m) prevents the entrainment and the ejection of macroscopic fuel or structure debris. The body of experience in accidents and experiments effectuated in the past confirms this point, provided that the water height above the core is significant.

The expansion of the vapour bubble is followed by a phase change at the vapour/liquid frontier. When the pressure significantly decreases, the water condenses and the bubble contracts itself to a new pressurized form before moving on to a new cycle. These oscillations continue, and the bubble rises up in its contracted phases, like in a submarine explosion.

The analysis of underwater explosions, carried out in the military domain in equivalent energetic conditions (equivalent TNT), showed that a chemical explosion does not produce a spray below 9m of water; merely a "dome", consisting of vertical water jets due to the cavitation phenomenon, is observed. As in a chemical explosion the totality of the bubble is formed by incondensable gas, the effects are intensified with respect to the steam explosion in terms of mechanics (no phase change), in terms of bubble cycle time (pulsations more frequent) and regarding the risk of entrainment of aerosol fuel particles (higher volume of incondensable gas).

This phase was also illustrated with the EXCOBULLE experiment [10] performed in the 1980's for breeder reactor needs. It aimed to study the behaviour of a hot drop in contact with a cold fluid, which takes place in three phases:

- a first, instable phase shows the exchange of hot liquid jets between the two phases (Rayleigh-Taylor instabilities develop at the exterior of the hot drop),

- a mixing phase, where the mixing zone becomes thin and can be describes as homogenous,
- a stable phase, where the condensing film is integrated in the steam bubble.

The bubble quickly disappeared after some oscillations, and change itself into a final smaller incondensable gas bubble.

Only the mechanical effects, essentially linked to the first expansion of the bubble (convective component of the shock wave), and the ascension of fuel aerosols via the incondensable gas are to be dreaded.

5 THE FUEL AND INCONDENSABLE GAS BUBBLE FUTURE

The fuel is ejected in the form of fine particles (some micrometers to some hundred micrometers), cooling down quickly in the water and falling down to the pool's floor. Thus a fraction of the fuel may be guided to the surface in aerosol form (diameter lower than 200 micrometers) within the incondensable gas bubble.

The analysis of experiments, performed in Japan at NSRR on RIA test [11] on comparable fuel plates and taking into account the statistical analysis of the fuel fabrication foreseen for the JHR, showed that less than 2% of the particles will have a size inferior to 70 µm after the accident. Only 12% of all particles can conservatively be considered as aerosols (d < 200 µm).

The gas bubble is essentially constituted of hydrogen (Al-water and NaK devices–water interactions), immediately formed during fuel-water interaction, and is quickly split into little fragments because of the structures within the core. The fuel particles are thus subjected to various physical phenomena during their slow rising within the instable cap-bubble form (figure 1): thermal-phoresis, diffusion-phoresis, coagulation, washing out, sedimentation (figure 2)…

Initially, and in a conservative approach, a model of aerosol sedimentation in a stable bubble (spherical of cap shaped) enabled a first analytic approach of the transport of aerosols ([12]). Using Stocke's law, the particles velocity can be expressed as a function of their size.

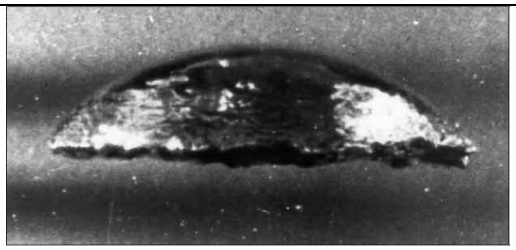

Figure 1 : Cap-bubble picture

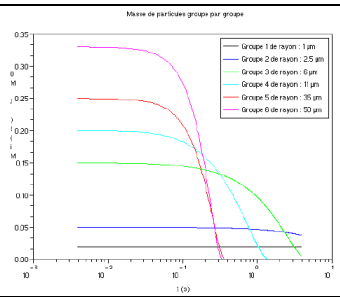

Figure 2 : Sedimentation model – Particles masses by group

The key results show that:

- Only bubbles with a diameter greater than 10 cm can transport aerosols to the surface, according to this simplified model; with a diameter in the range of 1 meter, a bubble can transport aerosol particles with a size up to 10 µm, thus carrying along a fraction of 0.2% of the transportable fuel aerosol particles (with 100% of the particles produced by the core in a lonesome bubble, and without washing out effect).
- No aerosol particle with a size of 20 µm or more will reach the surface of the pool (for bubbles with a diameter from 2 mm to 1.2 m or equivalent diameter for cap bubbles)

In conclusion, after first analysis, the sedimentation and the washing out are the essential phenomena because of the particle size distribution of the aerosols and the existing vapour in the bubble. These effects show a very significant return of the aerosols in the water.

In a second time, considering the convective effect in a bubble in contact with water, it appeared to be necessary to characterise better the behaviour of this kind of bubble (with a relatively significant size), in order to know if it would ascent to the pool surface without being fragmented underway.

A conservative on-going calculation with the TRITON code [13] simulates incondensable gas bubble hydrodynamics, combined with a DSMC code [14] enabling to "sow" this bubble with a known particle population.

6 THE RADIONUCLIDES' PROCESS

Except this potential phenomenon of a direct rising of fuel particles to the pool surface, the core radionuclides ejected during the explosion may migrate from the fuel either directly to the confinement, or indirectly through the pool water. This is particularly the case of the rare gas and volatile fission products (iodine family) which are the main contributors to the effective dose outside the facility.

A first step is related to the pressure increase in the containment after the explosion and due to the residual power, but also with potential existence of fission gas directly expulsed into the containment, constituting a direct and immediate thermal source.

This pressure excursion is calculated with the HORUS/Sys calculation route, based on the CATHARE code [15].

At the same time, the ASTEC ([16] - figure 3), CERES [17] and GAZAXI [18] codes are respectively used to calculate the iodine transfer process to the containment and the contribution of the main radionuclides to the effective dose during their migration outside the containment. They are used to verify that the containment design covers the BORAX risk.

Figure 3 : ASTEC-Iode – Modelisation of the iodine transfer process

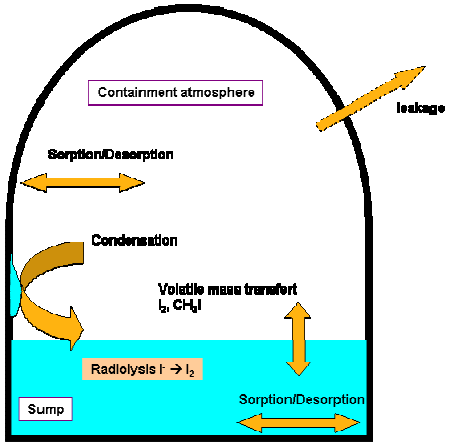

7 THE POOL SYSTEM AND VESSEL MECHANICAL CONSEQUENCE

The pressure wave created by the explosion propagates into the pool water up to the wall and ground, generating a characteristic impulse on the surfaces after multiples rebounds. This impulse may damage the material constituting the pools system (iron pool liner and wall concrete).

The EUROPLEXUS [19] and RADIOSS [20] codes (figures 4 and 5) are used for a quantitative evaluation of the reasonably conservative consequences of the BORAX accident in terms of the mechanical behaviour of the reactor structures.

Figure 4 : EUROPLEXUS pool and canal meshes

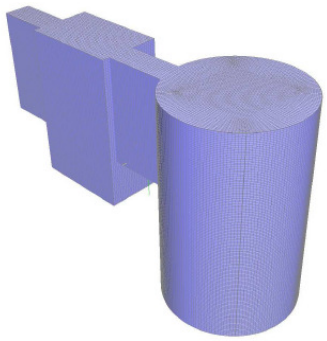

Figure 5 : RADIOSS modelling of concrete wall- 3D model

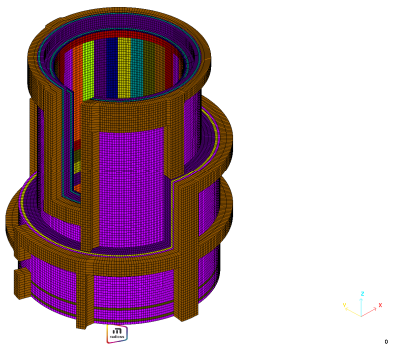

8 CONCLUSION – THE BORAX CALCULATION SCHEME FOR JHR

On the base of an active and constructive collaboration between the CEA and external units, a calculation scheme of the BORAX accident (figure 6) is under development, and will lead to:

- better understand the complex physical phenomena involved in very short time frames,
- obtain a reasonably conservative quantification of the different parameters at all stages of the accident,
- support safety assessment.

Figure 6 : BORAX calculation scheme

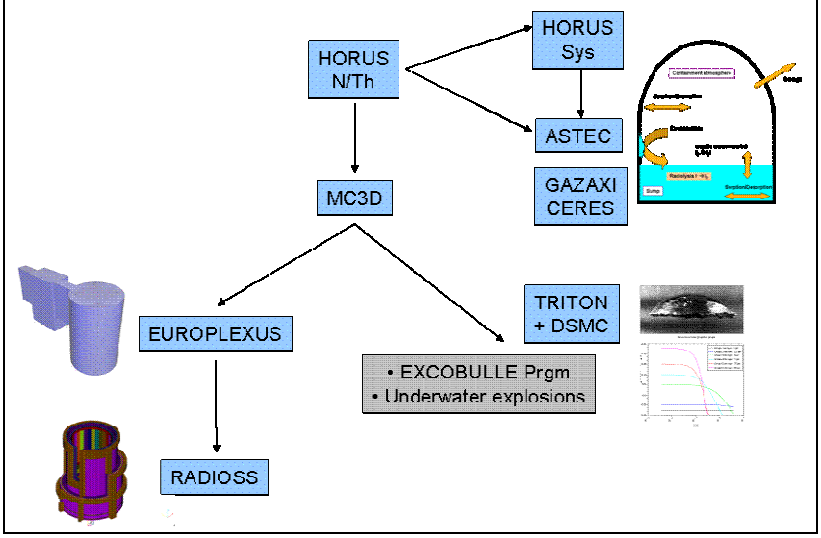

REFERENCES

[1] P.Trémodeux, X.Bravo, JP.Dupuy, G.Ithurralde, G.Perotto, "Jules Horowitz Reactor General lay out, main design options resulting from safety options, technical performances and operating constraints", TRTR2005-IGORR10, septembre 2005, Gaithersburgh, Maryland, USA

[2] J.J. Lautard et al., "CRONOS2 : a modular computational system for neutronic core calculations", IAEA meeting, Cadarache, France, 1990

[3] S. Aniel et al., "FLICA4: Status of numerical and physical models and overview of applications", NURETH 11, Avignon, October 2-6, 2005

[4] G. Willermoz et al., "HORUS3D : A consistent neutronics/thermohydraulics code package for the JHR modelization", ENC 2002, Lille, France

[5] C. Döderlein et al., "The 3D neutronics scheme for the development of the Jules Horowitz Reactor", PHYSOR 2008, Interlaken, Switzerland

[6] R.Sanchez, J.Mondot, Z.Stankovski, A.Cossic, and I. Zmijarevic, 1992. “APOLLO2 : A User-Oriented, Portable, Modular Code for Multigroup Transport Assembly Calculations”, Nuclear Science and Engineering, 100, pp. 352-362

[7] E. Royer, I. Toumi, “CATHARE-CRONOS-FLICA coupling with ISAS : a powerful tool for nuclear studies”, ICONE-6, May 10-15, San Diego, 1998

[8] B. Roussel, « Notice du code DULCINEE » (IPSN internal report)

[9] R.Meignen, G.Ratel, G.Berthoud, S.Picchi, “MC3D V5 –Description of the physical models of the explosion application”, (IRSN internal report)

[10] M.Amblard, G.Berthoud, J.Carré, A.B.Reynolds, G.Sims “The EXCOBULLE experiments on the expansion of large two-phase bubbles”, Nuclear engineering and design 61, 1980, (459-468)

[11] T.Fuketa, K.Ishijima, T.Fujishiro, K.Soyama, H.Ichikawa, T.Kodaira, “Fuel melting and mechanical energy generation during power burst experiments with aluminium-cladding uranium silicide fuel plate” - JAERI Research 95-077

[12] O.Grégoire, P.Salvatore, « Modèle simplifié de sédimentation des particules radioactives dans une bulle au cours de sa montée dans la piscine du réacteur », (CEA internal report)

[13] G.Allaire, S.Clerc, S.Kokh, “A five equation model for the simulation of interfaces between compressible fluids”, J.Comput. Phys. 181 (2002) 577-616.

[14] G.A.Bird, “Molecular Gas Dynamics and the Direct Simulation of Gas Flows”, Clarendon Press, Oxford, 1994

[15] M. Robert, M. Farvacque, M. Parent, and B.Faydide, “CATHARE 2 V2.5: A fully validated CATHARE version for various applications”, NURETH-10, Seoul, South Korea, 2003

[16] H.J.Allelein, K.Neu, J.P.Van Dorsselaere, “European Validation of the Integral Code ASTEC (EVITA) – First experience in validation and plant sequence calculation”, Nuclear Engineering and design 235 (2005), 285-308

[17] M.Monfort, "Présentation de la plate-forme CERES destinée à l’évaluation des conséquences des rejets de radionucléides dans l’atmosphère." Journée SFRP, Les Codes de Calcul en Radioprotection, Radiophysique et Dosimétrie (2006), (http://www.sfrp.asso.fr)

[18] « Calculs d’impact radiologique d’un rejet par voie atmosphérique en situation accidentelle, formulaire du code GAZAXI », (CEA internal report 1998).

[19] “EUROPLEXUS - A Computer Program for the Finite Element Simulation of Fluid-Structure Systems under Transient Dynamic Loading”, User’s manual, Version in Development of June 4, 2008, (http://europlexus.jrc.ec.europa.eu/public/manual_html/index.html)

[20] “RADIOSS Theory Manual”, Sept. 2003 (http://www.altair.com)

M. Varvayanni, P. Savva, N. Catsaros
NCSR "DEMOKRITOS"
Institute of Nuclear Technology – Radiation Protection
PoB 60228, 15310, Aghia Paraskevi, Greece
melina@ipta.demokritos.gr, savvapan@ipta.demokritos.gr, nicos@ipta.demokritos.gr

M. Antonopoulos-Domis
School of Electrical and Computer Engineering
Aristotle University of Thessaloniki, Thessaloniki, Greece
domis@eng.auth.gr

Corresponding author
M. Varvayanni, *melina@ipta.demokritos.gr*

ABSTRACT

Irradiation of target materials for research purposes is an everyday activity in material testing reactors. The estimation of the gamma heating expected to be deposited on irradiated samples is basic safety issue. The GHRRC (Gamma Heating in Research Reactor Cores) code developed in NCSR Demokritos, is based on a point-kernel parameterization. It includes the photons produced from U235 thermal fission and from (n,γ) reactions in the core materials. It uses empirical correlations for the dose build-up in the core and the energy absorption build-up in the irradiated sample. The dose build-up factor, as well as the macroscopic cross sections of U235 fission and (n, γ) reactions are determined assuming a homogenized core. In this work, GHRRC is used to estimate the relative importance of the mechanisms contributing to the total gamma heating of the irradiated material, for two different fuel enrichments in U235. Comparison is made between the gamma heating components produced in a core fuelled with a) Low Enrichment Uranium (LEU, 19.75% U235, 62.48g U per fuel plate) and b) High Enrichment Uranium (HEU, 93% U235, 10.8g U per fuel plate), with 13% burn-up. In both cases a critical core is considered, with the configuration of the Greek Research Reactor (slab geometry, pool type, light water moderated and cooled, beryllium reflectors, 34 fuel assemblies). The gamma heating of a small Fe sample, located in the middle of a central irradiation channel of the core is examined and the heating components considered are those due to a) the prompt and delayed fission gammas, b) capture gammas originated from heavy nuclides, fission products, structural materials and water and c) the gamma dose build-up in the core. For the capture gammas from fuel plate, indicative isotopes were examined (i.e. isotopes of U, Pu and Sm), based on the relative importance of their absorption macroscopic cross section and the data availability for their photon capture spectra. It was found that the higher thermal neutron flux of the HEU core causes higher heating from fission gammas than in the LEU core. However, the higher uranium content in LEU fuel makes the dose build-up more important in the LEU core. Also, the higher U238 content in LEU fuel induces more significant heating by capture gammas from U and Pu isotopes. The Si contribution (existing only in LEU) is found of small importance while the contributions of water, structural materials and fission products are found higher in the HEU core.

1 INTRODUCTION

Heating from gamma radiation of irradiated sample materials is an issue of primary importance for the safety and the radiation protection of research reactors. Designing of the optimum conditions for a sample irradiation requires calculation of the energy that will be deposited on the target material.

The GHRRC (Gamma Heating in Research Reactor Cores) is a “home-made”, three-dimensional numerical code, developed to estimate the gamma heating of small samples inside a research reactor core. The code, based on a point-kernel parameterization, was found to give reasonable gamma heating estimations within reasonable error margins, which allow the Reactor Operator to pre-determine the irradiation conditions so that the sample temperature will safely remain below the melting point during irradiation [1].

In the present work, GHRRC is used to estimate the relative importance of the mechanisms contributing to the total gamma heating of an irradiated Fe sample, for two different fuel enrichments in U235, with 13% burn-up. The results show that the higher thermal neutron flux in the high enrichment (HEU) core causes higher heating from fission gammas than in the low enrichment (LEU) core. However, the higher uranium content in LEU makes the dose build-up more important in the LEU core. Also, the higher U238 content in LEU induces more significant heating by capture gammas from U and Pu isotopes. The Si contribution (existing only in LEU) is found of small importance while the contributions of water, structural materials and fission products are found higher in the HEU core.

The aim of this work is a) to present the capability of an easily handled model to reasonably assess the relative importance of the components of the gamma heating deposited in a sample irradiated in a research reactor core and b) to contribute to the studies performed within the framework of the RERTR (Reduced Enrichment for Research and Test Reactors) Program [2].

2 THE GHRRC CODE

As mentioned above, GHRRC code is a three-dimensional numerical code, based on a point-kernel parameterization.

The developed model includes the prompt and delayed photons produced from the U235 fission and the gammas produced by neutron capture ((n,γ) reactions) in the core materials. Empirical correlations are adopted for the dose build-up in the core and the energy absorption build-up in the irradiated sample. The required neutron fluxes are calculated using the neutronics code system XSDRNPM [3] and CITATION-LDI2 [4] in a three-dimensional representation of the Greek Research Reactor (GRR-1) core. For the determination of the macroscopic cross sections for the U235 fission and the (n,γ) reactions in the core materials, a homogenization of the core is performed. The attenuation coefficient of the monoenergetic γ-rays is also derived for a homogenized core, as a with-respect-to-density weighted sum of the individual attenuation coefficient values of the core materials [5]. The same approximation is used for the derivation of the core dose build-up factor based on the values tabulated for each core material.

Thus, the rate of the total gamma energy deposited per unit volume of the sample is computed from:

$$W = \int_{V_c} \int_{E} w(\vec{r}, E) dE d\vec{r}_0 \quad (1)$$

Where E is the photon energy, V_c is the core volume and $w(\vec{r},E)$ is the heat deposited per unit volume of the sample irradiated at position $\vec{r}$, from the monoenergetic gamma rays E released at core position $\vec{r}_0$. In the GHRRC $w(\vec{r},E)$ is computed from:

$$w(\vec{r},E)dE = dE\ \frac{\mu_{ab}(E)}{\bar{\ell}\mu_{at}(E)}\left(1-e^{-\mu_{at}(E)\bar{\ell}}\right)$$
$$B_s(\mu_a(E)\bar{\ell},E)B_c(\mu(E)|\vec{r}-\vec{r}_0|,E)E\,\frac{e^{-\bar{\mu}(E)|\vec{r}-\vec{r}_0|}}{4\pi|\vec{r}-\vec{r}_0|^2}d\vec{r}_0\sum_n A_n(\vec{r}_0,E)\Phi_n(\vec{r}_0) \quad (2)$$

Where $\mu_{at}(E)$ and $\mu_{ab}(E)$ (in [cm^{-1}]) are respectively the attenuation and the absorption coefficient of the monoenergetic photons of energy E in the sample material, $\bar{\ell}$ is the mean chord length of the sample defined as $\ell = 4Vs/Ss$ with V_s and S_s being respectively the volume and total surface of the sample [6], B_s is the build-up factor for the energy absorption in the sample material, B_c is the dose build-up factor in the homogenized core, $\bar{\mu}(E)$ is the attenuation coefficient of the photons of energy E in the homogenized core, $\Phi_n(\vec{r}_0)$ is the neutron flux at core position $\vec{r}_0$ for neutron energy group n and A_n is given from the relationship:

$$A_n(\vec{r}_0,E) = \sum_j \Sigma_{j,n}(\vec{r}_0)Y_{j,n}(E) + \Sigma_{f,n}(\vec{r}_0)X_n(E) \quad (3)$$

Where, $\Sigma_{jn}(\vec{r}_0)$ (in [cm^{-1}]) is the macroscopic cross section of (n,γ) reaction for nuclide 'j', with neutrons of the energy group 'n' at core position $\vec{r}_0$, $Y_{jn}(E)$ (in [J^{-1}]) is the spectrum of gamma rays of energy E due to (n,γ) reactions in nuclide 'j', with neutrons of the energy group 'n', $\Sigma_{f,n}(\vec{r}_0)$ (in [cm^{-1}]) is the fission macroscopic cross section of neutron energy group 'n' at the core position $\vec{r}_0$ and $X_n(E)dE$ is the probability that a photon of energy between E and $E+dE$ results from fission-produced neutron at the energy group 'n'. In GHRRC, for $X_n(E)dE$ exponential fits are used [7], [8] while for $Y_{j,n}(E)$ the discrete values of PGAA-IAEA and NNDC databases have been included [9], [10].

It should be noted that in the present model application only the gamma rays produced from reactions (fission and capture) with thermal neutrons have been considered, due to lack of gamma rays yield data from epithermal neutrons reactions.

In GHRRC, the energy integration is performed using the trapezoidal method, while a 21-Point, 5th-degree of accuracy formula for triple integrals is used for the volume integration [11].

The code is capable of calculating the gamma heating components separately, with respect to the different reaction types, i.e. fission, core built-up and capture. The code can be very easily handled, even by poorly experienced users.

3 MODEL APPLICATION TO THE GRR-1 CORE

GRR-1 is a pool type, light water moderated and cooled reactor, using beryllium reflectors and fueled by MTR-type fuel elements. The reactor is normally operating at 5MW power. The active core dimensions in x, y (horizontal) and z (vertical) directions are 45.66cm, 47.74cm and 62.55cm respectively. There are five control blade locations in the core where shim/safety rods are placed. Two critical core configurations were used in this work. In the

first one only low enrichment uranium fuel was considered (LEU, 19.75% U235), containing 62.48g U per fuel plate. In the second one only high enrichment uranium fuel was considered (HEU, 93% U235), with 10.8g U per fuel plate. In both cases the U235 burn-up was 13%. The horizontal core configuration is shown in Figure 1, using x (letters) and y (numbers) coordinates. The grid position D4 hosts a control fuel assembly without control rod and is used as a flux trap. Grid positions D4, A7 and F7 are used for material irradiation.

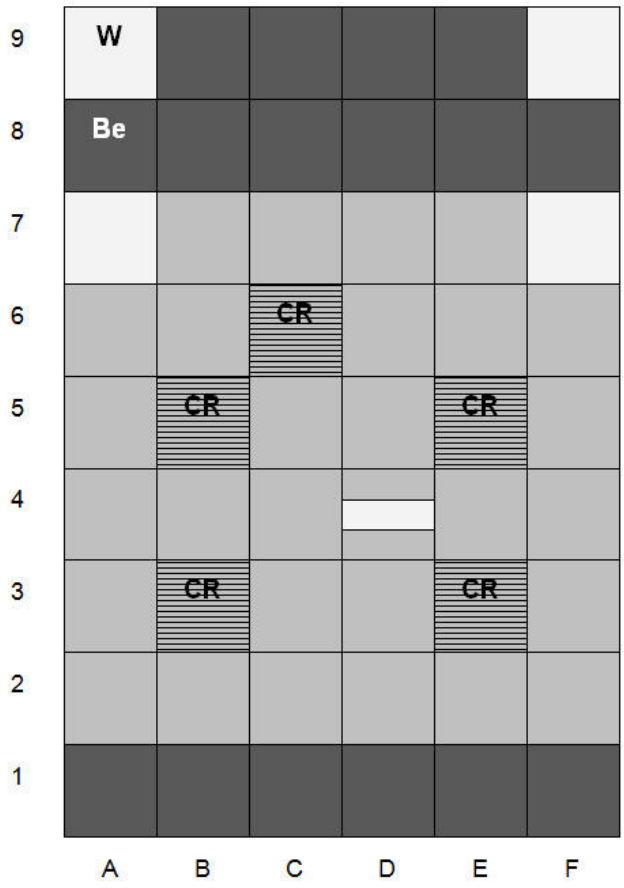

Figure 1**:** Horizontal cross section of the GRR-1 Core. The notation is: **CR** for control fuel assemblies with control rods inserted, **W** for water and **Be** for beryllium reflectors.

The gamma heating of a Fe cylindrical sample of 5cm height and 0.7cm diameter, placed in the middle grid channel D4 was calculated using GHRRC. The heating components considered in the computations include (i) prompt and delayed fission gammas, (ii) capture gammas originated from heavy nuclides, fission products, structural materials and water and iii) the gamma dose build-up in the core and the energy absorption build-up in the sample. For the capture gammas from fuel plate, indicative isotopes were examined (i.e. isotopes of U, Pu and Sm), based on the relative importance of their absorption macroscopic cross section and the data availability for their photon capture spectra.

It should be noted that the beryllium blocks and the surrounding pool water were not considered, since their homogenization with the active core that intervenes between the considered volume and the irradiated sample in D4, would introduce more significant error than their omission. Also, the γ-rays produced from thermal capture in several nuclides that are present in the irradiated fuel plates were not taken into account, since their (n,γ) spectra were not available. Thus, less than 25% of the above nuclides was taken into account, while nuclides with significant (n,γ) cross section in the thermal range, such as Xe135, Sm151, Pu241, Pm isotopes and others, were omitted.

The computational domain includes the core shown in Figure 1, with 20cm of surrounding pool-water in all six sides. The three-dimensional group-averaged neutron flux in the GRR-1 core as well as the densities of the nuclides contained in the irradiated fuel inventory were calculated using the neutronics code system XSDRNPM and CITATION-LDI2 with the NDF5 238-group library; a slab geometry with the actual nuclide distribution was considered for the above calculations, i.e. separate homogenized zones were defined in the core, as in [12], [13]. Five neutron energy groups were considered, the thermal threshold being at 0.5 eV. The macroscopic cross sections of the U235 fission and the (n,γ) reactions in the core materials, Σ_f and Σ_j respectively, were determined assuming a homogenized core, through the relationship:

$$< \Sigma_c >= \frac{\sum_{i=1}^{nz} \sigma_{j,i} N_{j,i} V_i}{V_c} \quad (4)$$

where $< \Sigma_c >$ stands for Σ_f or Σ_j, nz is the number of homogenized zones that include the nuclide j (e.g. for a nuclide of the fuel meat, nz is equivalent to the number of fuel assemblies), $\sigma_{j,i}$ is the equivalent microscopic cross section (fission or capture) of the nuclide j in the zone i, $N_{j,i}$ is the number density of the nuclide j in the zone i, V_i is the volume of zone i and V_c is the volume of the active core, i.e. without beryllium blocks and surrounding pool water.

4 RESULTS AND DISCUSSION

The results are shown in Table 1. As can be seen, the higher thermal neutron flux of the HEU core causes higher heating from fission gammas than in the LEU core. However, the higher uranium content in LEU makes the dose build-up factor more important in the LEU core, thus resulting to a higher total power density deposited in the sample from fission in the LEU than in the HEU core. Also, the higher U238 content in LEU induces more significant heating by capture gammas from U and Pu isotopes. The Si contribution (existing only in LEU) is found of small importance while the contributions of water, structural materials and fission products are found higher in the HEU core. Aluminium contribution, in particular, is higher in HEU due to its higher content in the HEU meat.

It should be noted that the results in Table 1 are expected to be underestimated, due to (a) the omission from calculations of heating mechanisms such as inelastic scattering, activation of nuclides, epithermal capture and thermal capture in several core compartments and fuel plate nuclides and (b) the core homogenization at least for the core materials that are not really distributed in the core, such as the control rod constituents. The omission of the pool water and the beryllium blocks may have caused higher underestimation of the total gamma heating in the LEU core, since the build-up of the gamma rays that travel towards the sample is expected more significant in LEU. On the other hand, the omission of (n, γ) reactions in several nuclides of the irradiated fuel may have induced higher underestimations either in the LEU or the HEU case, depending on the omitted nuclide. For example, the omission of Pu isotopes is expected to cause more significant underestimation to the LEU result, while the omission of (n, γ) in fission products, such as Xe, Pm and some Sm isotopes, is expected to cause gamma heating underestimation in HEU. However, it should be noted that the results are considered comparable in the two fuel enrichments.

Table 1: Gamma Heating Power Density deposited in a Fe sample from several mechanisms, for two different fuel enrichments in U235

Gamma heating component	**W_c (W/cm^3) LEU**	**W_c (W/cm^3) HEU**
Non Built-up Fission	8.89	10.85
Built-up Fission	15.56	15.08
Core-buildup factor	1.75	1.39
Capture U	0.035	0.008
Capture Al	0.732	0.825
Capture Pu	0.454	0.00012
Capture H	0.542	0.595
Capture Sm	0.0308	0.0324
Capture Si	0.0152	0.000
Total γ-Heating	17.369	16.540

5 CONCLUSIONS

GHRRC is a three-dimensional numerical code for gamma heating computations, based on a point kernel parameterization, which was developed in NCSR "Demokritos". The code, which is very flexible and easily handled, is capable of calculating the gamma heating components separately, with respect to the different reaction types, i.e. fission, core built-up and capture.

In this work, GHRRC was applied to two different core configurations (LEU, 19.75% U235, 62.48g U per fuel plate and HEU, 93% U235, 10.8g U per fuel plate) of the Greek Research Reactor (GRR-1). The gamma heating power density deposited in a Fe sample located in the middle of a central irradiation channel of the core was computed. Comparison of the gamma heating between the two configurations showed that the higher thermal neutron flux of the HEU core causes higher heating from fission gammas than in the LEU core. However, the higher uranium content in LEU makes the dose build-up more important in the LEU core. Also, the higher U238 content in LEU induces more significant heating by capture gammas from U and Pu isotopes. The Si contribution (existing only in LEU) is found of small importance while the contributions of water, structural materials and fission products are found higher in the HEU core, due to higher neutron fluxes. The omission from the code of surrounding materials, such as the reactor pool water and the beryllium blocks, may have caused underestimation of the total gamma heating, which is higher in the case of LEU core, since the build-up of the gamma rays that travel towards the sample is expected more significant in LEU. On the other hand, the omission of (n, γ) reactions in several nuclides of the irradiated fuel have induced underestimations which might be higher either in the LEU or in the HEU core, depending on the omitted nuclide. However, the results are considered comparable for the two fuel enrichments, a finding that can be very useful in cases of core conversion studies, since the transition from a HEU to a LEU core does not seem to yield safety issues rising from the gamma heating.

REFERENCES

[1] M. VARVAYANNI , N. Catsaros and M. Antonopoulos-Domis, "Gamma heating of irradiated samples in a research reactor" (2007). http://nestoras.ee.auth.gr/reports/GammaHeatingModel.pdf

[2] Reduced Enrichment for Material and Test Reactors, http://www.rertr.anl.gov.html

[3] N. M. GREENE and L. M. Petrie, "XSDRNPM A one-Dimensional Discrete-Ordinates Code for Transport Analysis", Oak Ridge National Laboratory, ORNL/NUREG/CSD-2/V2/R6 (2000).

[4] T. B. FOWLER, D. R. Vondy and G. W. Guningham, "Nuclear Reactor Core Analysis Code: CITATION", Oak Ridge National Laboratory, ORNL-TM-2496, Rev. 2 (1971).

[5] E. P BLIZARD, "Nuclear Radiation Shielding", Ann. Rev. of Nucl. Sci. 5, 73-98 (1953).

[6] J. J. DUDERSTADT and L. J. Hamilton, "Nuclear Reactor Analysis", J. Wiley & Sons Inc., New York (1976).

[7] F. C. MAIENSCHEIN, "Prompt-fission gamma rays. In Engineering Compendium on Radiation Shielding, Volume1: Shielding Fundamentals and Methods", edited by R. G. Jaeger, E. P. Blizard, A. B. Chilton, M. Grotenhuis, A. Honig, Th. A. Jaeger and H. H. Eisenlohr (Springer-Verlag, Berlin, Heidelberg, New York) (1968a).

[8] F. C. MAIENSCHEIN, "Fission product gamma rays. In Engineering Compendium on Radiation Shielding, Volume1: Shielding Fundamentals and Methods", edited by R. G. Jaeger, E. P. Blizard, A. B. Chilton, M. Grotenhuis, A. Honig, Th. A. Jaeger and H. H. Eisenlohr (Springer-Verlag, Berlin, Heidelberg, New York) (1968b).

[9] PGAA-IAEA Database for Prompt Gamma-ray Neutron Activation Analysis, http://www-nds.iaea.org/pgaa/

[10] NNDC database Thermal Neutron Capture γ's (CapGam), http://www.nndc.bnl.gov/capgam

[11] G.W. TYLER, "Numerical integration of functions of several variables", Canad. J. Math. 5, 393-412 (1953).

[12] M. VARVAYANNI, E. Stakakis, N. Catsaros and M. Antonopoulos-Domis, "Void induced reactivity in a mixed MTR core" Nucl. Eng. And Des., 235, 855-865 (2004).

[13] M. VARVAYANNI, D. Grigoriadis, N. Catsaros and E., Stakakis, "Neutronic calculations for the conversion to LEU of a research reactor core" RERTR 2007 International Meeting, Prague, September 23-27 (2007).

Data Collection Computerized System for TRIGA Research Reactor

Daniela Mladin
Institute for Nuclear Research Pitesti
Campului, PO.Box 78, Mioveni, 115400, Romania
daniela.mladin@nuclear.ro

ABSTRACT

The data collection for TRIGA SSR 14 MW reactor started in the frame of co-ordinated IAEA research project "Up-date and expand IAEA Reliability Database for research reactors for PSA use". The necessity to develop a raw data collection and processing computerized system arose due to the need to:

- Store all the information regarding the events produced in the operation of TRIGA SSR reactor, whether these are systems or components failures, events due to test or maintenance or information about reactor power, time intervals, number of scrams, etc.;
- Identify, retrieve, select and group information from raw data sources in a time interval period;
- Calculate reliability data, failure data and confidence interval limits, which are used as input data in the Probabilistic Safety Analysis for TRIGA Research Reactor;
- To study the failure rate evolution for the components.

The paper presents the Computerized System called "PSARelData", which is used to manage raw data for the history of failures, to obtain reliability data in the PSA analysis and to give information about failure trends. The system was developed in the Visual Basic 6.0 programming environment. The interfaces of Visual Basic 6.0 with Windows Access and Windows Excel allowed to develop the database and to calculate the failure rates and confidence interval limits (95%, 5%) using statistical functions.
The computerized system includes operation events for TRIGA SSR 14 MW reactor during 1979 – 2000, covering three data sources: Shift Supervisor Reports, Reactor Logbooks, Work Authorizations.

1 INTRODUCTION

The data collection for TRIGA Steady State Reactor 14 MW reactor started in the frame of coordinated IAEA research project "Up-date and expand IAEA Reliability Database for research reactors for PSA use" [1]. In the frame of the CRP mentioned above more than 40 components were analysed and processed according to the boundaries and failure modes selected. Generally, the components investigated belong to different systems of TRIGA SSR reactor. More than 6.000 failure and related maintenance records were considered during data collection. Not only independent failure but multiple components failures susceptible to CCF were also collected. In case of multiple components, the events collected are analyzed with respect to component type, failure mode and failure degree. These events involved pumps, control rods and control rod drives, funs, valves. Qualitative analysis of root causes, coupling factors, corrective actions and quantitative analysis of the events were performed. The

information regarding raw data was stored in MS EXCEL worksheets. The period of data collection was chosen between 1979 and 2001 involving three data sources: Reactor Log Books, Shift Supervisor Reports and Maintenance Work Authorizations. Due to necesity to store all the information regarding events in the operation of TRIGA 14MW reactor and to perform reliability data analysis, a software application was created after the completion of the IAEA CRP mentioned. The system for data collection and processing offers a software which may be used in raw data collection, in making queries in the database and in reliability data calculation.

The paper presents a brief description of the Computerized System, developed for TRIGA SSR 14 MW reactor and some conclusions refering to this system.

2 DESCRIPTION OF COMPUTERIZED SYSTEM

2.1 Brief description of logic diagram for data computerized system

The Computerized System called "PSARelData" is used to manage raw data for the history of failures, to obtain reliability data and use them further, in the PSA analysis. Also, the PSARelData system, developed in the Visual Basic 6.0 programming environment gives information about failure trends for different reactor components and structures in different failure modes. The interfaces of Visual Basic 6.0 with Windows Access and Windows Excel allow to develop the database and to calculate the failure rates and confidence interval limits (95%, 5%) using statistical functions [2]. The logic diagram used for the computerized data system is presented in the Figure 1. Information regarding the failure data, test and maintenance data, number of scrams, etc, is collected from the three above mentioned raw data sources of TRIGA research reactor and is available for processing. By the processing action one obtains a visualization of all the failure records ordered in time, or just a selection of these. In addition, the processing of data may go on with the calculation of failures rates and confidence intervals limits. The visualization is possible on the screen but paper reports can be produced, too.

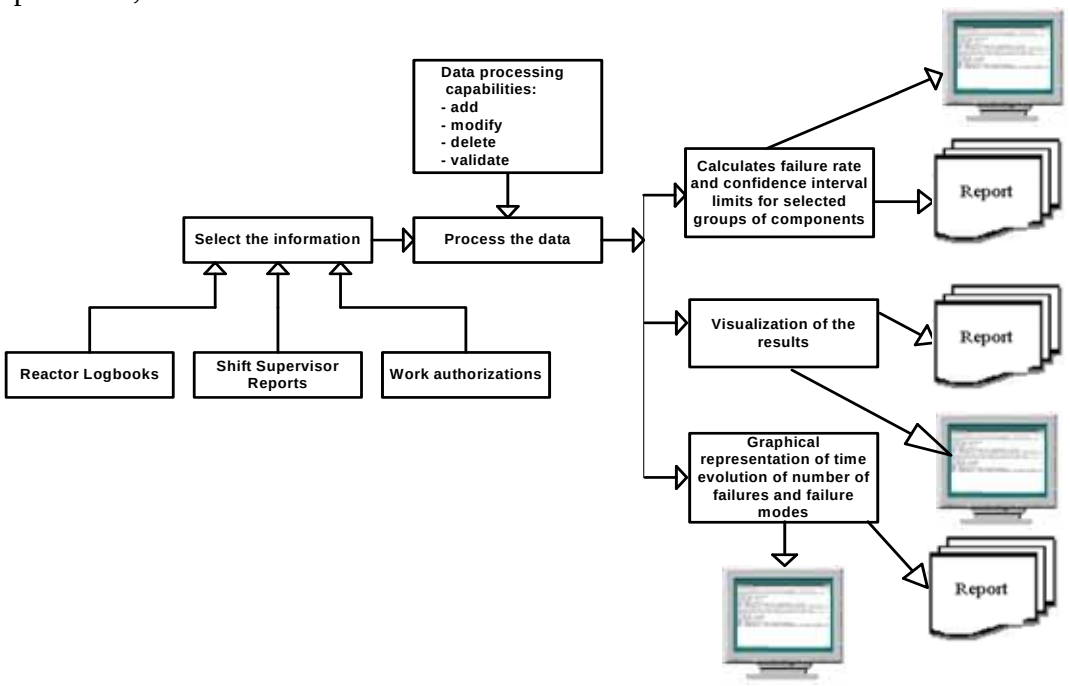

Figure 1: Logic diagram for data Computerized System

2.2 Brief description of the computerized application

The computerized application contains five screens (forms). The main form of the application (Figure 2) gives the view of the whole database and offers the possibility to navigate inside it. By means of the main form it is possible to introduce new data and to edit the already existing records using the corresponding buttons.

The component type and failure modes (including critical and degraded failure modes) were taken from IAEA TECDOC 930 and in connection with available information from TRIGA data sources. The event type criteria include the following possibilities: functioning, reparable, revision, replaced, verification.

Also, from the main form one can switch to the queries form (enlarged main form), which allows one to impose different simultaneous criteria for data grouping and selection. The selection criteria are:

- name of the component
- starting and ending dates of the requested failure time interval
- component type
- system to which component belongs
- failure mode
- operation mode (run or stand-by).

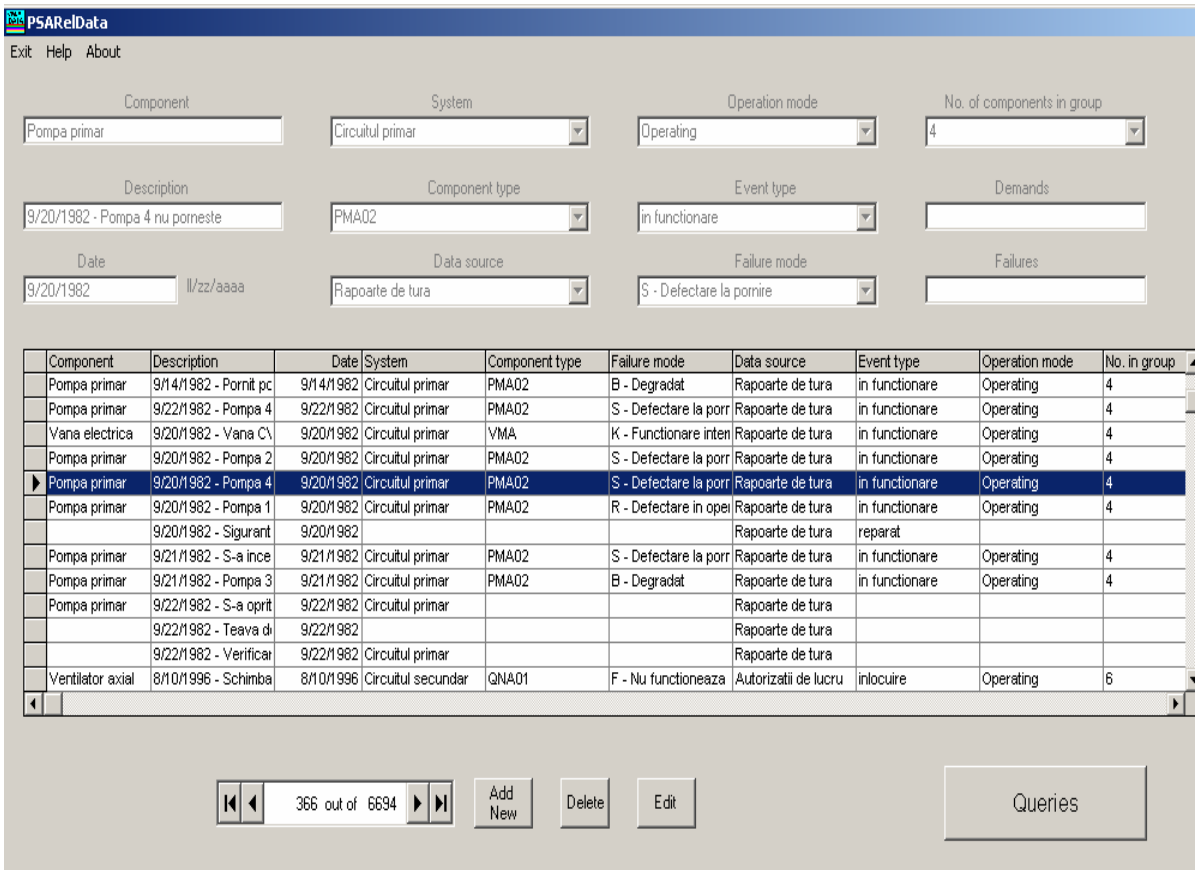

Figure 2. Main form of the application (with example records in Romanian)

From the enlarged main form is also possible to write a report containing the result of selection process and to calculate the failure rate or failure probability (depending on the operation mode: run or stand-by) according to statistical formulas. This calculation is accompanied by the calculation of confidence interval limits and the results are displayed in a new view of the datagrid in the enlarged main form. The computerized system calculates failure rate and confidence interval limits for the components in two operation modes: run and stand-by.

To calculate the interval limits, Excel functions are used for F distribution and chi-square distribution according to [3]. The formulas are as follows:

Stand-by

If f is the number of failures and d is the number of demands, then:

Probability: $p = \frac{f}{d}$ (1)

Lower 5% limit: $p_l = 1/(1+(d-f+1)/f * FINV(0.05, 2*(d-f+1), 2*f))$ (2)

, where $FINV$ is probability fraction of cumulative F-distribution from EXCEL

Upper 95% limit: $p_u = 1/(1+(d-f)/(f+1)/FINV(0.05, 2*(f+1), 2*(d-f)))$ (3)

Note that f and d are sums of "Failures" and respectively "Demands" fields content over all records appearing in the queries datagrid for that stand-by component.

Operating

If n is the number of failures, dt is the effective (operation) time interval and N is the number of identical components in group then:

Failure rate: $\lambda = n/dt/N$ (hr^{-1}) (4)

Lower 5% limit: $\lambda_l = CHIINV(0.95, 2*n)/2/dt/N$ (5)

, where $CHIINV$ is inverse of chi-square (χ^2) distribution from EXCEEL

Upper 95% limit: $\lambda_u = CHIINV(0.05.2*(n+1))/2/dt/N$ (6)

Note that n is taken automatically as the number of failure records appearing in the queries datagrid for that operating component.

The application is asking for the ratio (R) between the operation time and calendar time (C). The later is taken as a date difference function between ending date and starting date. The failure rate is calculated using the effective (operation) time interval in hours:

$dt = R \times C$

The time ratio (R) is less or equal with 1.00 (pre-defined value = 1.00).

The output of the calculation is displayed as a new grid view containing the six or seven fields (depending on the operation mode) bearing the following column captions:

- ✓ “Component”
- ✓ “Component type”
- ✓ “Failure mode”
- ✓ “Failure rate (hr^{-1}) for operating components or probability for stand-by components”
- ✓ “Lower limit for confidance interval limit 5%”
- ✓ “Upper limit for confidance interval limit 95%”
- ✓ “Time used to calculate lambda (h)” (only for operating components).

To restore the queries datagrid view from the lambda calculation output view, the “Show selected records” button can be used.

The figures 3, 4 and 5 show the results of the selection process and calculation of failure rates for two components (centrifugal cooling fan and control rod drive).

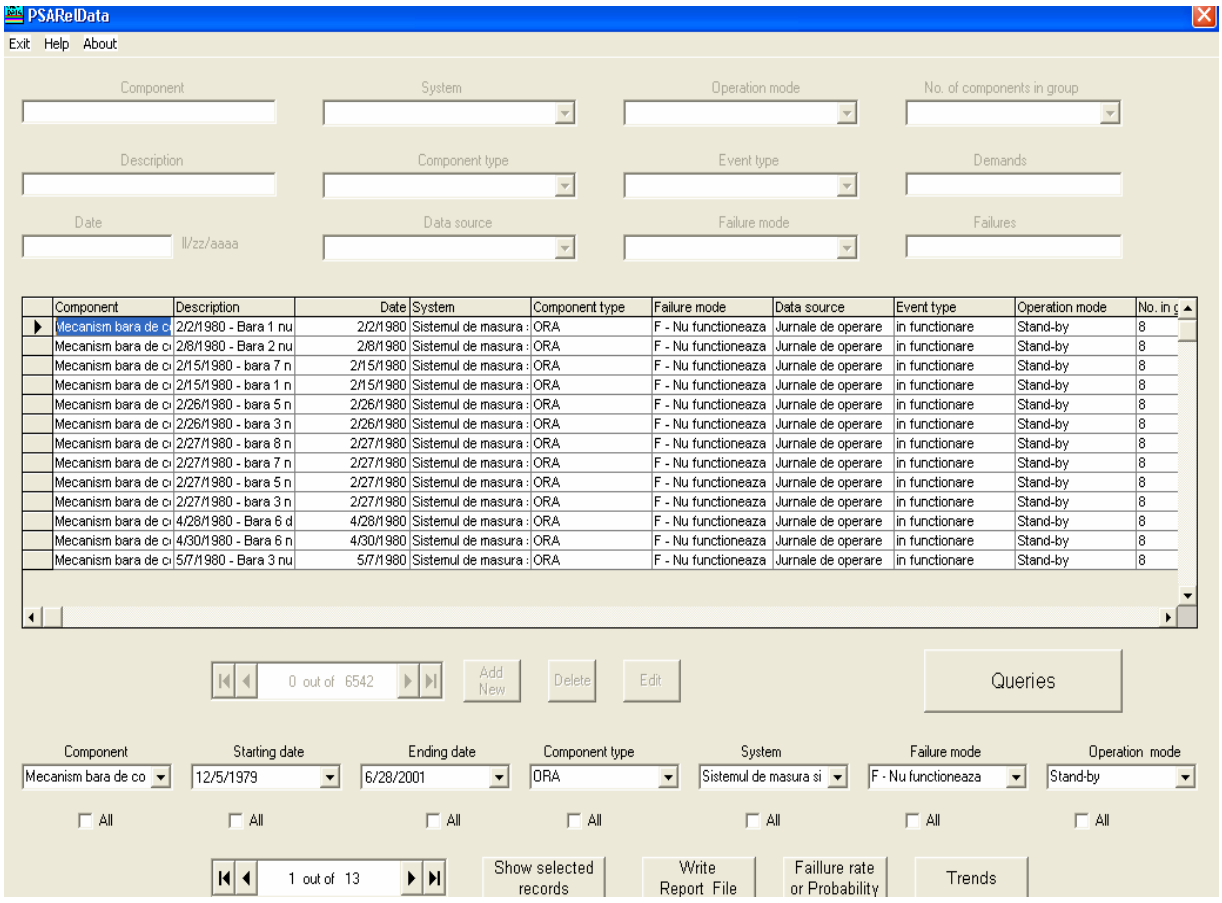

Figure 3. Selection process results for a component in stand-by (control rod drive) for failure rate calculation

The operation mode for the selected failure examples is different for the two cases: centrifugal fan – run mode and control rod drive – stand-by mode.

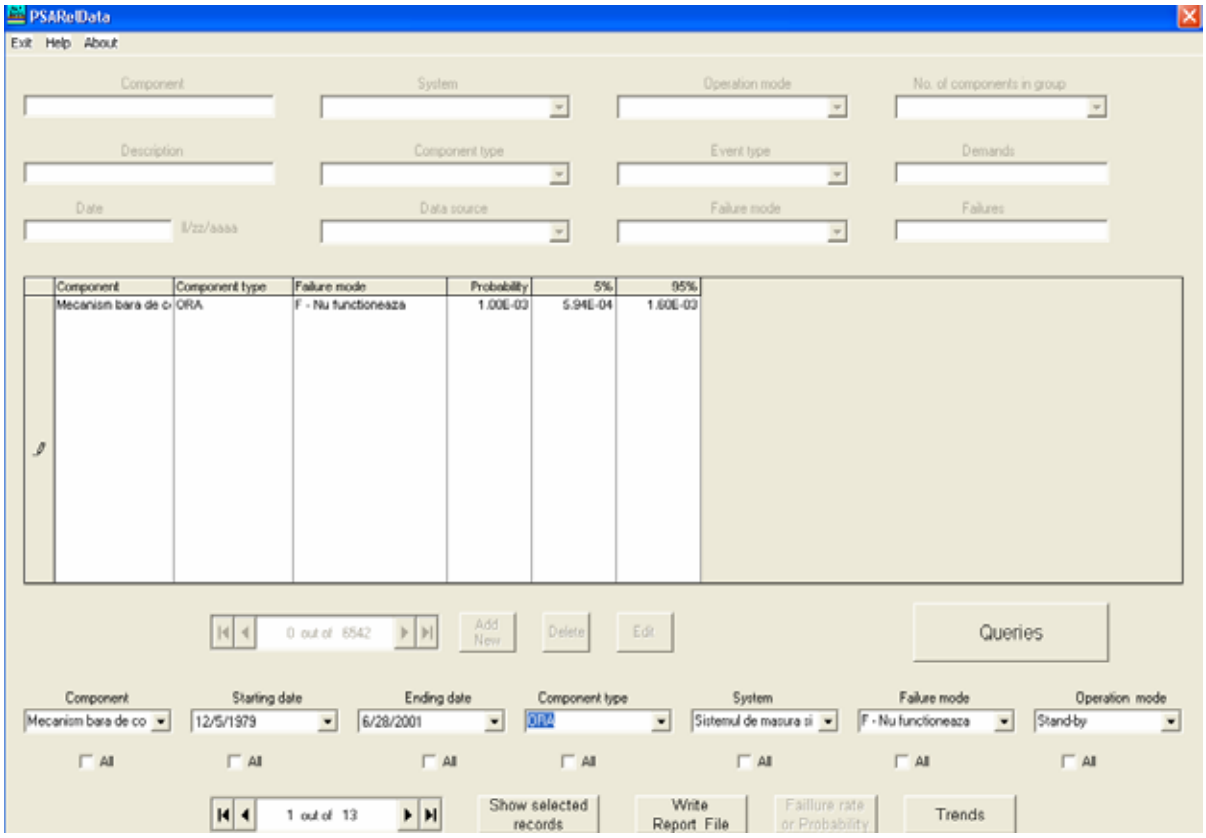

Figure 4. Results of calculation of failure rate and confidence interval limits for control rod drive (stand-by mode)

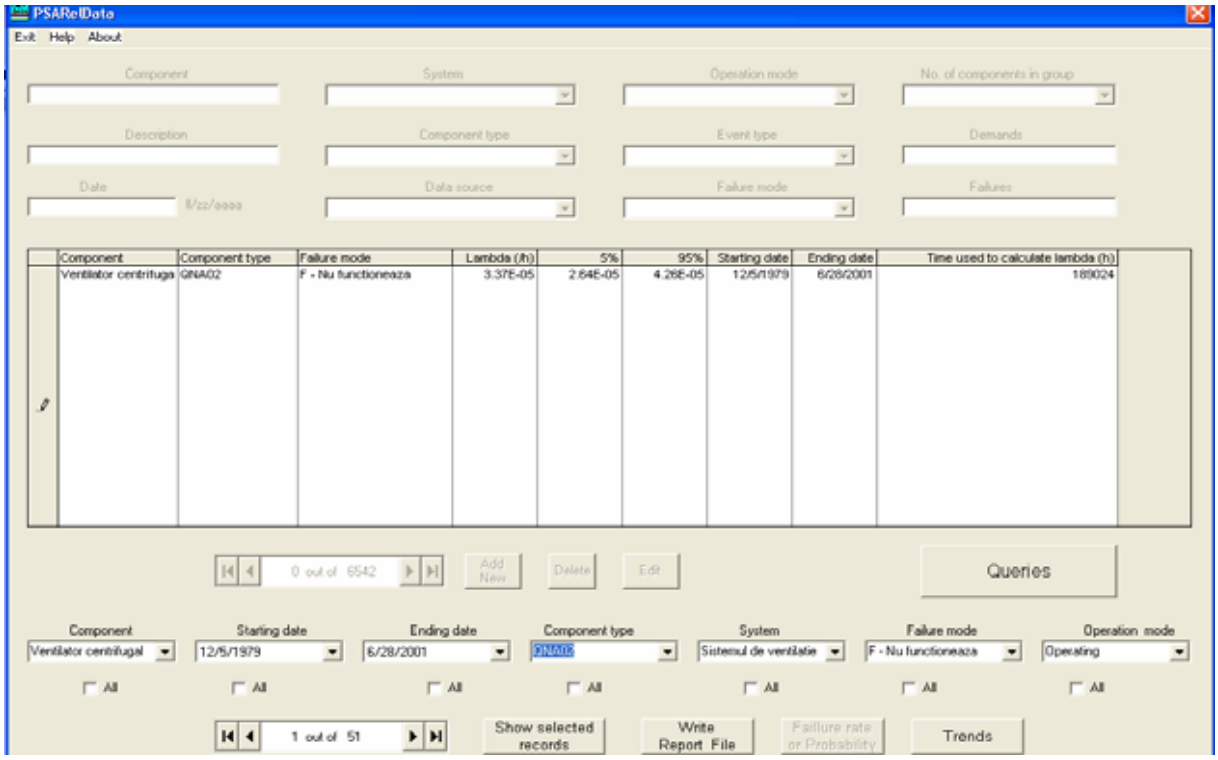

Figure 5. Calculation results of failure rate and confidence interval limits for the centrifugal fan (operating mode)

The application has two auxiliary forms that deal with supplementary data in case the “Data source” field in the database is either “Work Authorizations” or “Reactor Logbooks” (figure 6 and figure 7). In these cases, the auxiliary forms, appearing automatically, allow the recording and editing of the particular data that are found for that failure event in each of two data sources.

The “Work Authorization” form appears automatically at click event on Validate data button in order to record additional data when the data source is “Work Authorizations”.

The data can be edited by means of text boxes, except for the first two fields which are displayed here for the sole purpose of identifying the failure record and consequently they cannot be modified at this stage. Thus only the Starting data, Starting hour, Ending date and Ending hour are to be introduced and/or modified using the controls in this form.

This additional form includes a data control that can be used to navigate through all the records in the database having the data source “Work Authorizations” and to determine the position of the current record inside this particular collection.

There is also a “Write Report File” button which causes the ‘Report_File1.txt’ to be written in the working directory.

The “OK” button will update the database and send the application back to the current edited record in the main form datagrid.

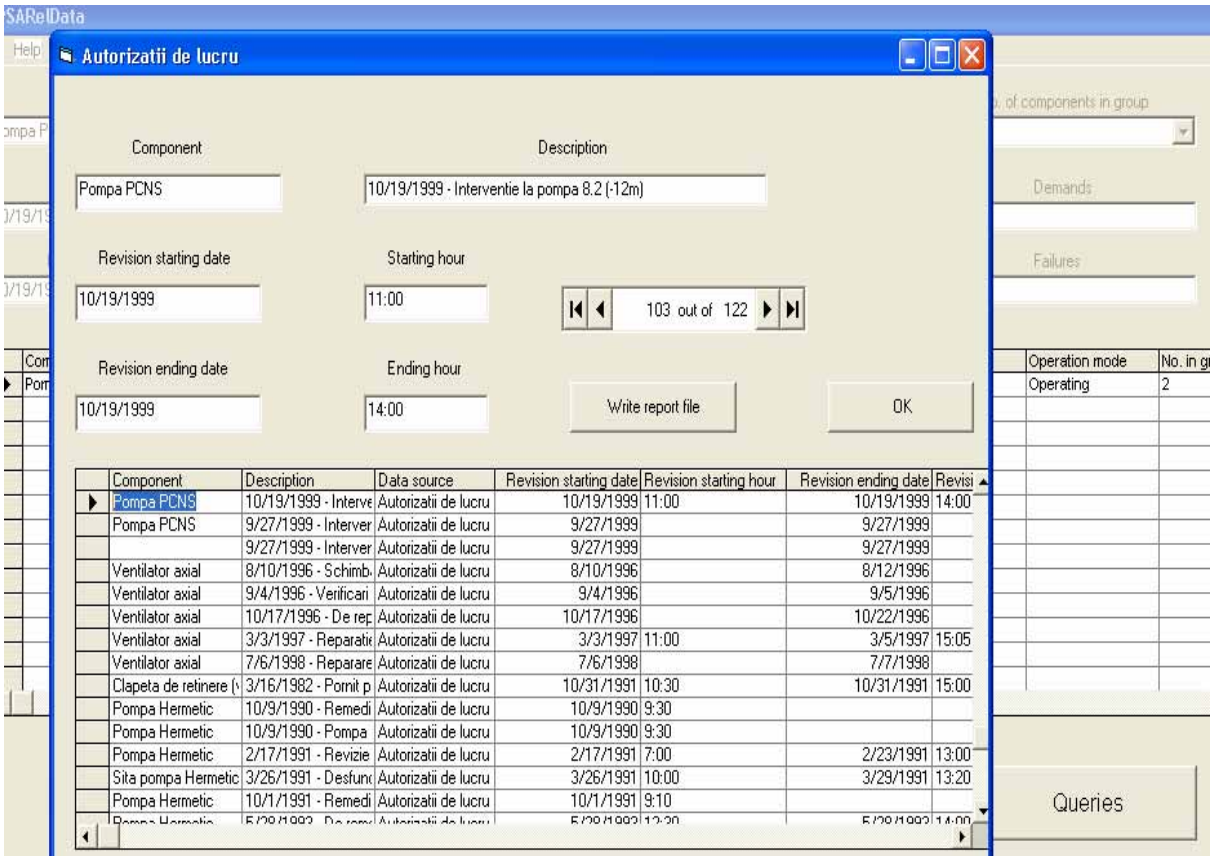

Figure 6. Auxiliary form for “Work Authorizations” data source

The “Reactor LogBooks” form appears automatically at click event on Validate data button in order to record additional data when the data source is “Reactor LogBooks“.

The data can be edited by means of the text boxes. In the case of “Reactor LogBooks” form, the first two fields cannot be modified at this stage. Thus only the reactor starting date, starting hour, number of control drives fail up, reactor shutdown date, shutdown hour, reactor shutdown mode, number of control drives fail down, time interval are to be introduced and/or modified using the controls in this form.

This additional form includes a data control that can be used to navigate through all the records in the database having the data source “Reactor LogBooks” and to determine the position of the current record inside this particular collection.

There is also a Write Report File button which causes the ‘Report_File2.txt’ to be written in the working directory.

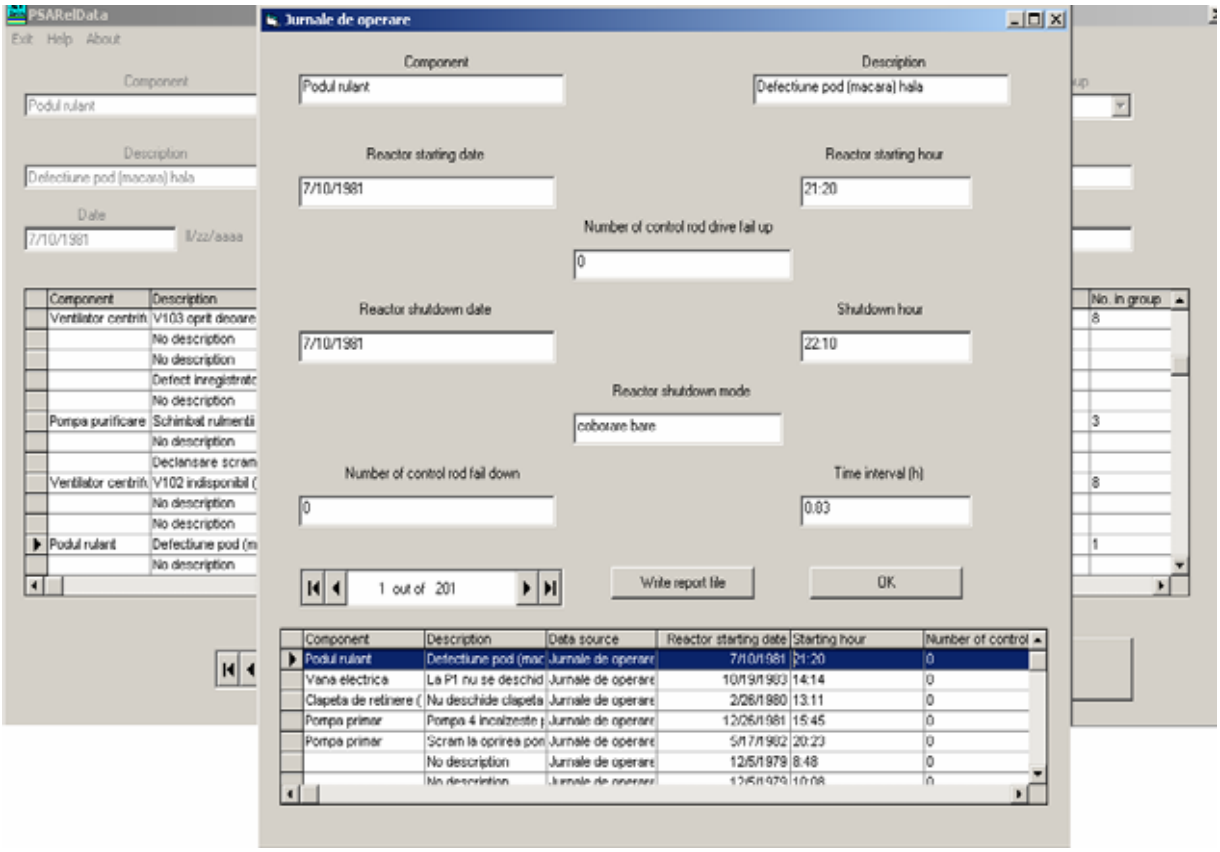

Figure 7. Auxiliary form for “Reactor Logbooks” data source

The application has the capability to represent graphically the time evolution of number of failures and failure rate by dividing the chosen time interval in an equal number of segments also defined by the user. The form appears on click event on “Trends” button. The time interval, between the starting date and ending date, is divided according to user defined number of time division which is introduced in the coresponding form. Selection can be made using the “Line/Bar” check box for the representation of either 2D bars chart type or line chart type.

“Copy” button permits the copy of chart type or line chart type in a word file, using the “Paste special” from the menu of Word.

Example of time evolution of “Fail to run” failure mode for TRIGA main pumps failure rate is shown in the figure 8.

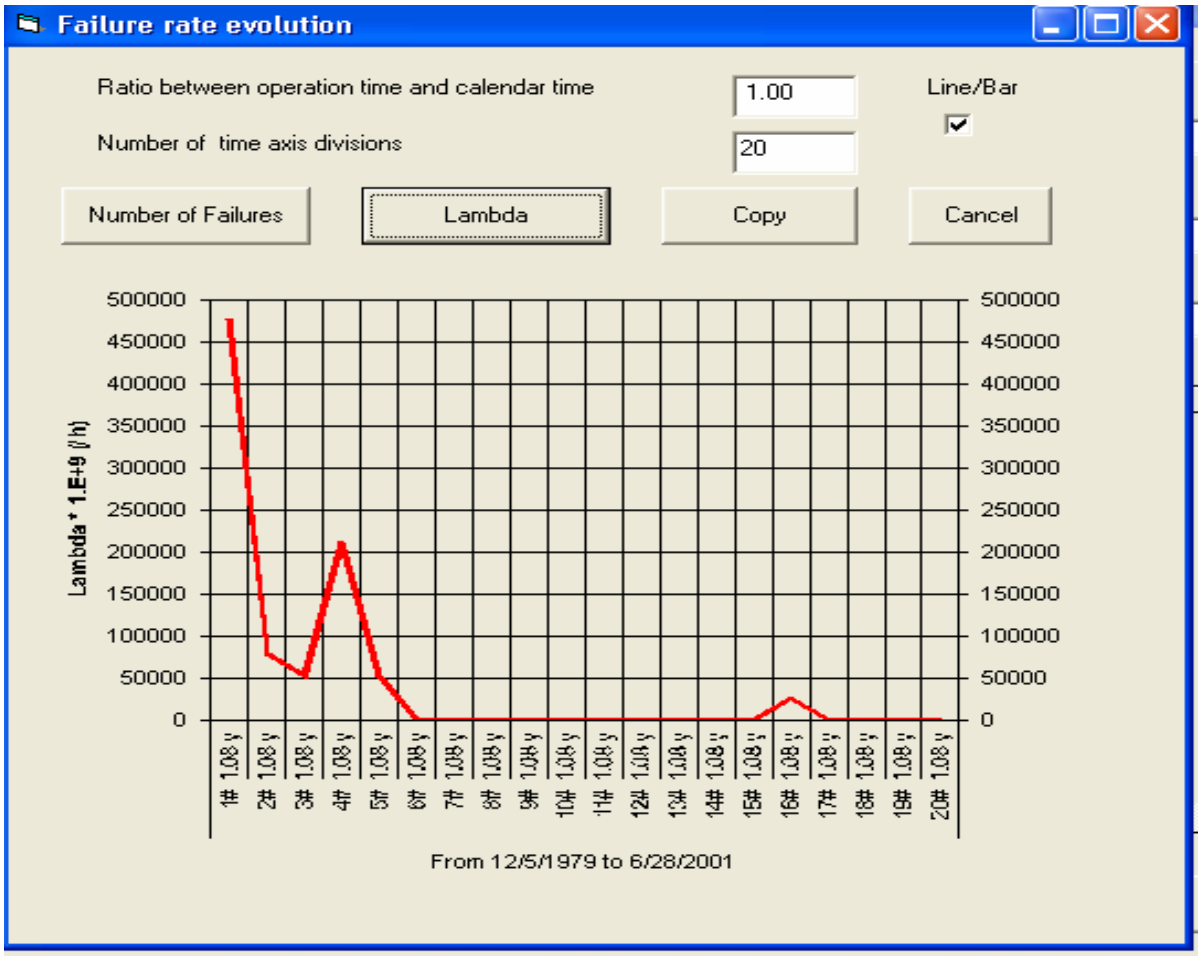

Figure 8. Example of time evolution of TRIGA main pump failure rate for “Fail to run” mode

3 CONCLUSIONS

The necessity to develop a raw data collection and processing computerized system arose due to the need to:

- Store all the information regarding the events produced in the operation of TRIGA SSR reactor, whether these are systems or components failures, events due to test or maintenance or information about reactor power, time intervals, number of scrams, etc.;
- Identify, retrieve, select and group information from raw data sources in a time interval period;
- Calculate reliability data, failure data and confidence interval limits, which are used as input data in the Probabilistic Safety Analysis for TRIGA Research Reactor;
- To assist maintenance, test activity in order to have a schedule of these activities, to optimize the test intervals, repair times;
- To study the failure rate evolution for the components.

The PSARelData System can be applied successfully with minor modification not only for the others Research Reactors but also for data collection in the NPPs.

ACKNOWLEDGMENTS

The author is grateful to the TRIGA Reactor Department in INR for their collaboration in raw data collection for TRIGA SSR 14 MW Reactor.

REFERENCES

[1] D. MLADIN, “Contribution of TRIGA 14 MW reactor to the reliability database for research reactors PSAs as part of Coordinated Research Programme:” Update and expand the IAEA Reliability data for RRs for PSA use”, Final Reports, 2001-2004.

[2] D. MLADIN, “Data collection Computerized System for TRIGA Reactor,” Internal report no 7805 (in Romanian), Institute for Nuclear Research Pitesti, Romania, september 2007

[3] IAEA – TECDOC-636 – Manual of reliability data collection for research reactor PSAs

TOPSAFE
Dubrovnik, Croatia, 30.09 - 3.10.2008

Safety Barriers for the HANARO Research Reactor

HoanSung Jung, InCheol Lim
Korea Atomic Energy Research Institute
1045 Daedukdaero, Yusunggu, Daejeon city, KOREA
hsjung@kaeri.re.kr, iclim@kaeri.re.kr

ABSTRACT

The HANARO, a 30MW pool type research reactor in KOREA, has many safety barriers to prevent accidents or to mitigate the consequences of accidents. Multiple barriers are incorporated into the design to avoid core damage, irradiation accidents, and a release of radioactive material and a leakage of pool water. Safety barriers designed by considering a defence-in-depth concept should always be operable. The integrity of these barriers are verified periodically by tests and inspections. The reactor operation is restricted according the operating limiting conditions if any barrier is broken. In this paper, hazards and safety barriers are discussed.

1 INTRODUCTION

The HANARO is a pool type research reactor which produces a 30MW thermal power and a maximum 5E14 thermal neutron flux maximum. The reactor assembly consists of an inlet plenum, a heavy water tank with a honeycomb shape core, and a hexagonal chimney. The reactor uses light water as a coolant for all cooling system and heavy water for the reflector cooling system. There are three water pools in the reactor hall of the reactor building. The reactor pool and the spent fuel pool are 13 meters deep to attain a sufficient shielding and cooling capacity and the service pool is 6 meters deep. The reactor hall acts as a confinement which allows a limited leakage of air. Many safety barriers are incorporated into the design of the HANRO for a health, physical, industrial, radiation, and nuclear safety.

2 SAFETY BARRIERS

2.1 Physical and Industrial Safety

The environment in the reactor hall is not void of the accidents which are common in industrial plants. There are water pools, deep rooms with removable hatches, high walk ways, and cranes as shown in figure 1.

Figure 1 View of the reactor hall

For the potential dangers in the reactor hall, the countermeasures are provided in the table 1.

Table 1 Barriers against the physical and industrial hazards

Hazards	Area	Barriers	Verification
Falling(human, things)	-Pool -Walkway -Crane -Deep room	-Safety hand rail -Access control	-Surveillance -Supervising
Dropping(things)	-Pool -Walkway	-ditto -deposit	-ditto -training
Sabotage	-Hall and building entrance	-Safety door -Finger print identification -Multiple check points	-Periodic tests -Supervising -Audit
Dangerous work	-Work place	-Personal protective equipment -Proper tools -Human error protection	-Work procedure -Training

2.2 Radiation Safety

All the nuclear facilities in HANARO have mitigation provisions for the relevant postulated accidents to protect humans, the environment, and equipment. Because HANARO is a pool type reactor, shielding and cooling is maintained by the inventory of the pool water. And the heavy water is managed strictly to avoid the risks from a tritium leakage. The air contaminated in the reactor hall is filtered and exhausted through the dedicated ducts and stacks to reduce risks to the employee, the public, and the environment. Also the solid and

liquid wastes are collected in a defined way and moved to a waste management facility in a controlled manner. Barriers provided for the radiation protection are presented in table 2.

Table 2 Barriers against radiation hazards

Hazards	Risks	Barriers	Verification
-Pipe break -Seal leakage	-Loss of pool inventory	-High connection pipe -Siphon hole	-Periodic inspection
-Pool liner leakage	-Loss of pool inventory	-Concrete shielding -Stainless steel liner -Leak detector	-Periodic inspection -Real time monitoring
-Beam tube leakage	-Loss of pool inventory	-Leak-tight joint -Leak detector -Leak-tight tube cover	-Periodic inspection -Real time monitoring
-Failure of dampers, filters, and ducts	-Loss of confinement function	-Redundant devices -Filter performance -Monitoring sensors -D2O equipment room confinement	-Periodic tests -Performance tests -Real time monitoring (position, pressure difference)
- Waste spread	-Failures of waste management	-Administrative control -Proper equipments -Check points	-Work permit -Periodic inspection -Surveillance -Supervising
-Contamination	-Failure of work control	-Administrative control -Work procedure -Monitor and survey	
-Irradiation	-Accidents	-Biological Shied -Administrative control -Work procedure -Human error protection	-Barrier verification -Work permit -Safety evaluation -Safety culture -Supervising -Real time monitoring -Sampling and analysis

2.3 Nuclear Safety

Nuclear safety, such as a core damage protection is a basic and important feature for nuclear installations including the HANARO reactor facility. Safety barriers for the nuclear hazards of the HANARO reactor are provided by considering the relevant postulated initiating events. The following events are analysed and verified as manageable events within a safe shutdown state

- Loss of a coolant flow
  - Loss of a primary coolant flow
  - Loss of electric power
  - Failure of a bypass flow control
  - Loss of a secondary coolant flow
  - Loss of a reflector coolant flow
- Reactivity accidents
  - Start-up accident

- Withdraw of control rods
- Reactivity insertion from the experimental facility
- Introduction of cold water

- External events
  - Earthquake
  - Fire
  - Flooding
- Other failures
  - Fuel handling
  - Equipment failure

All the relevant postulated events or accidents can be mitigated to prevent core damage or a severe accident by the following multiple barriers

- Fuel design
- Fuel cladding
- Upward and passive cooling system
- Reactor concrete island
- Pool water inventory
- Biological Shield
- Confinement building
- Emergency ventilation system
- Emergency water supply system
- Reactor protection system
- Fail safe design

3 CONCLUSIONS

Hazards in the HANARO research reactor facility are investigated. There are risks to a physical, industrial, radiation, and nuclear safety in the HANARO plant. Multiple barriers for the various hazards are provided in the form of physical installations, work procedures, and administrative measures. In addition to the barriers, many training programs cover the potential human errors.

REFERENCES

[1] Safety Analysis Report for the HANARO Research Reactor, KAERI/TR-710/96, 1996, KAERI, KOREA

Transient Behaviour of Low Enriched Uranium Silicide Plate-Type Fuel for Research Reactors during Reactivity Initiated Accident

Kazuaki YANAGISAWA
Japan Atomic Energy Agency （JAEA）
1233 Watanuki, Takasaki, Gunma, 370-1292, Japan
yanagisawa.kazuaki@jaea.go.jp

ABSTRACT

The pulse irradiation tests were conducted on un-irradiated silicide mini-plate fuels. The principal aim is to study a failure threshold and its mechanism as a function of deposited energy and peak cladding surface temperature. It is revealed that the fuels were intact at energy depositions <82 cal/g but failed at energy depositions of >94 cal/g. A failure threshold must be existed between these two values. Two failure modes, that is, a through-plate cracking occurred below the melting point of Al cladding （640deg.C） and Al cladding melt above 640deg.C are revealed. The cause of the former is estimated to be a thermal stress occurred during fuel quench.

1 INTRODUCTION

To understand a transient behaviour of a low enrichment uranium silicide mini-plate fuel for material testing and research reactors, the experiment was conducted on un-irradiated mini-plate fuels at Nuclear Safety Research Reactor （NSRR）in JAEA （The former Japan Atomic Energy Research Institute, JAERI）. In 13 experiments, 8 mini-plate fuels were damaged at the temperatures ranged from 174 deg.C to 970 deg.C. Fuel failure threshold and failure mechanism as well as dimensional stability of the mini-plate fuel were studied by means of in-core instrumentations and post-pulse irradiation examination （PIE）. The results obtained in this study should be useful as a database for safety evaluation of water cooled research reactors existed in the world [1].

2 EXPERIMENT

2.1 Test Mini-Plate Fuel

The test mini-plate fuel used in this study were designed by JAERI and fabricated by two foreign vendors; CERCA in Romans, France and B&W in Lynchburg Virginia., the U. S. The outline of it is shown in **Fig. 1.** Similar plate-type fuels are fabricated for the cores of the Japan Materials Testing Reactor （JMTR） and Japan Research Reactor-3 （JRR-3）. The fabrication processes for these mini-plate fuels were described elsewhere [2,3]. Characteristics of the test mini-late fuel are summed up in **Table 1**. The test mini-plate fuel consists of the fuel core （25×70×0.51mm）sandwiched by Al-3wt%Mg based alloy cladding （35×130×0.38mm）, hereinafter abbreviated as “Al cladding”.

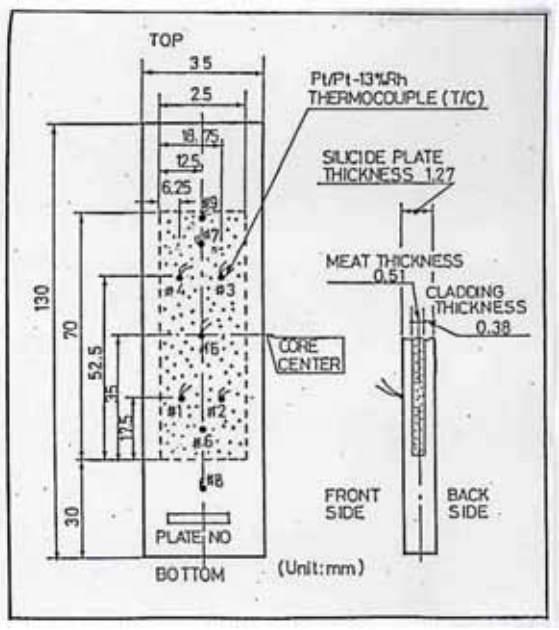

Figure 1: Schematic presentation of tested silicide mini-plate fuel having enrichment by 19.89 wt% ^{235}U and density by 4.8 g/c.c.

Table 1: Physical and mechanical parameters of the tested silicide mini-plate fuel fabricated by CERCA and B&W.

1. Silicide core (U-21wt%Al-7.5wt%Si)	
(1) Dimension (mm)	70 (length) x 25 (width) x 0.51 (thickness)
(2) Enrichment (wt%)	19.89 (0.84～0.86 gU-235 per plate)
(3) Element	
Si (wt%)	7.5 (CERCA), 7.7 (B&W)
U (wt%)	92.3, U density : 4.8g / c.c.
	Void fraction：5.0±0.9 (CERCA), 6.3±0.9 (B&W)
(4) Composition	
Fuel	U3Si2+USi, U3Si2 density :12g / c.c., U3Si2 > 97wt%
Matrix	A5NE (CERCA), A6061-0 (B&W)
2. Aluminum alloy cladding	
(1) Dimension (mm)	130 (length) x 35 (width) x 0.38 (thickness)
(2) Composition	Al-2.8wt%Mg-0.04wt%Mn-0.01wt%Cr (AG3NE)
	Al-1.0wt%Mg-0.67wt%Si-0.25wt%Cu-0.25wt%Cr (A6061-0)
(3) Density (g/c.c.)	2.67
(4) Mechanical properties	
at room temp.	CERCA B&W
Tensile strength (MPa)	240 114
0.2% proof strength (MPa)	130 62
Elongation (%)	25 29
(5) Blister test	No blister at annealing temperature of 475℃, >1h

2.2 Instrumentation and Irradiation Capsule

The in-core instrumentation was Pt/Pt-13%Rh bare wire thermocouples (0.2mm outer diameter), hereinafter abbreviated as "T/C's". Of which melting point was 1,780

deg.C. These were, as shown in **Fig. 1**, spot welded directly to the external surface of the mini-plate fuel at different locations. The maximum numbers of welded T/C's a mini-plate fuel were 9. In most experiments, however, T/C's used were 5. After assembling mini-plate fuel in the supporting jig with electric cables, it was loaded into irradiation capsules as shown schematically in **Fig. 2**. All the irradiation tests with those instrumentations were conducted in stagnant water at room temperature about 20 deg.C and one atmospheric pressure inside the sealed irradiation capsule [4].

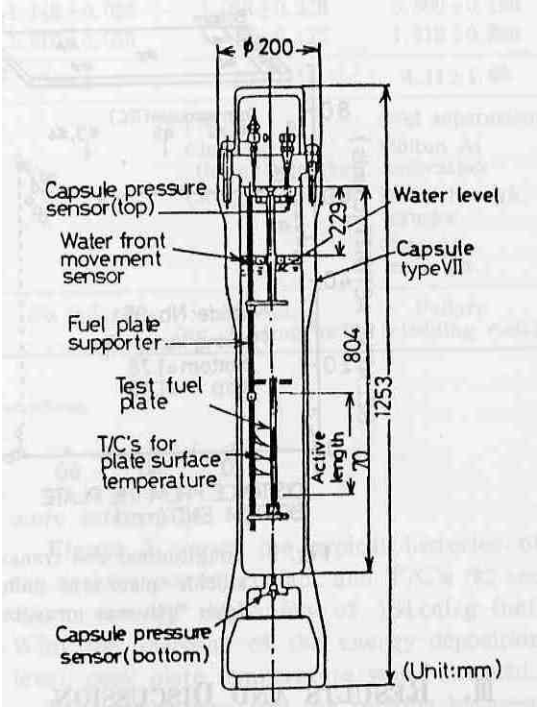

Figure 2: Schematic drawing of NSRR irradiation capsule for experimental series of 508 for the silicide mini-plate fuel.

2.3 Pulse history

The half-width of power of NSRR pulse irradiation is a minimum of about 4.4ms at a maximum integral power of 110MW・s. The value of this width varies from 4.4 to 20ms depending on the magnitude of inserted reactivity. The effect of pulse width variation in this experiment is, however, negligible since the pulse-width is far below the thermal time constant of the mini-plate fuel (approximately 0.1s). The integral value of the reactor power P （MW・s）measured by micro fission chambers was used to estimate deposited energy Eg （cal/g・fuel plate）in each test mini-plate fuel. Hence, Eg = kg × P, where the power conversion ratio kg （cal/g・fuel plate per MW・s）, is the ratio of mini-plate fuel power to reactor power. This ratio was determined through fuel burn-up analysis [5], taking the radial and axial power skew into consideration.

Table 2 : Summary of the results of in-core measurements and PIEs for the tested silicide mini-plate fuels

Experiment	508-12	508-1	508-2	508-10	508-7	508-9	508-6	508-8	508-11	508-13	508-3	508-4	508-5
Miniplate fuel number	CS514837	CS514815	CS514816	12907020	12907010	CS514834	CS514831	CS514832	CS514836	12907030	CS514819	CS514829	CS514830
Deposted energy (cal/g·fuel plate)	32	62	77	82	94	95	96	97	98	115	116	154	164
Peak cladding surfece temperature (°C)													
#1	133	x{a}	200	216	198	279	270	309	NoT/C	391	350	971	779
#2	136	177	179	180	210	315	229	261	-	-	372→387	893	689
#3	136	216	183	227	199	284	202	211	-	-	414	652	x
#4	134	234	178	173	237	285	x	244	-	-	393	881	918
#5	139	178	195	204	191	305→261{b}	205	330	-	-	424→544	930→957	578→656
#6	139	{c}-	-	182	-	280	-	-	-	-	-	-	-
#7	140	-	-	173	-	282	-	-	-	-	-	-	-
#8 (No active fuel core region)	60	-	-	-	-	-	-	-	-	-	-	-	-
#9	135	-	-	-	-	-	-	-	-	-	-	-	-
Average±σn-1(°C)	137±3	201±28	187±10	194±22	207±18	290±14	227±31	271±48	-	391	418±74	871±128	761±117
Coolant temperature; prepulse (°C)	21	20	22	21	24	22	21	24	21	16	18	17	22
; peak (°C)	26	24	26	28	53	58	43	45	39	42	47	35	34
Temp.drop ΔT(Tmax-Tp); min (°C)	26(#1, #5)	72(#5){d}	77(#2)	73(#1,#4)	74(#5)	149(#7)	96(#3)	105(#3)	-	391(#1)	240(#1)	540(#3)	463(#2)
; max (°C)	31(#9)	128(#4)	98(#5)	129(#3)	122($4)	202(#2)	159(#1)	214(#5)	-	391(#1)	440(#5)	882(#1)	853(#4)
Cladding wall; min (mm)	0.256	0.320	0.261	0.355	0.340		0.347	0.330	0.355	0.347	0.154	0.000{e}	0.010
Cladding wall; max (mm)	0.412	0.419	0.388	0.413	0.408		0.416	0.412	0.427	0.394	0.540	0.671	0.652
Fuel meat thickness; min (mm)	0.433	0.426	0.427	0.462	0.450	No PIE	0.423	0.442	0.427	0.491	0.447	0.565	0.578
Fuel meat thickness; max (mm)	0.556	0.610	0.587	0.543	0.554		0.558	0.560	0.549	0.554	0.620	1.078	1.125
Fuel plate thickness; min (mm)	1.235	1.270	1.148	1.240	1.206		1.233{f}	1.224{f}	1.247	1.261	1.058	0.560	0.795
Fuel plate thickness; max (mm)	1.253	1.330	1.21	1.260	1.274		1.258	1.261	1.267	1.289	1.440	1.515	1.549
Maximum bowing (mm)	0.22±0.14	None	None	0.11±0.07	0.12±0.11		0.53±0.16	0.14±0.07	0.11±0.03	0.43±0.38	1.2±0.85	6.4±0.18	2.7±1.2
Failure(F) / No Failure (NF)	NF	NF	NF	NF	F	F	F	F	NF	F	F	F	F
Faikure mode					Mechnical crcking due to thermal stress							Cladding melt	
Findings in PIE{g}					IC(2),PT(2)	PT(3)	IC(1)PT(1) HS(1)	IN(1),PT(1) HS(1)		IC(1),PT(1)	IC(3)	PT(2) CS, CM	IC(1), PT(1) CS, CM

{a} Thermocouple (T/C) malfunctioned
{b} Two temperature peaks
{c} No thermocouples(T/C's) welded
{d} Temperature drop of 72°Cocurred due to quench at thermocouple location #5
{e} No cladding wall due to significant aluminun agglomeration and denudation
{f} Thickness reduction due to hot apot was not taken into consideration
{g} IC:Incipient crack(number of observations), PT: Through-plate crack, HS: Hot spot, CS: Fuel core separation, CM: Aluminum cladding melt

3 RESULTS AND DISCUSSION

3.1 Transient Temperature

Table 2 is the summary of the results of in-core measurements and PIE. Technical terms used in the table are explained in the following sections.

In **Fig. 3**, a typical transient temperature measured by T/C #4 that received an energy deposition of 97 cal/g・fuel plate is shown with the pulse power, indicated by dotted line. It can be seen from the figure that cladding surface temperature（hereinafter abbreviated as CST） exceeded the boiling temperature, T_i （154 deg.C）, beyond the saturation temperature, T_{sat} （100 deg.C）, due to the pulse irradiation. Commencement of coolant boiling at temperature T_i was determined by data from capsule water level sensor. Namely, the timing of coolant boiling was detected by the movement of water free surface, and the timing of water free surface movement is detected by floating buoy having a magnetic sensor . The CST continued to increase to an overshoot temperature, T_{ov} （203 deg.C）. It then decreased to 194 deg.C and remained <10ms. This CST was thought to be the commencement of film boiling. The author signify it as T_{DNB} and denote here as the departure from nucleate boiling （DNB） temperature. A signal of DNB temperature can be detected from a temperature plateau should be appeared after T_{ov}. The DNB value was found to be 174±6 deg.C from the average of 31 data points.

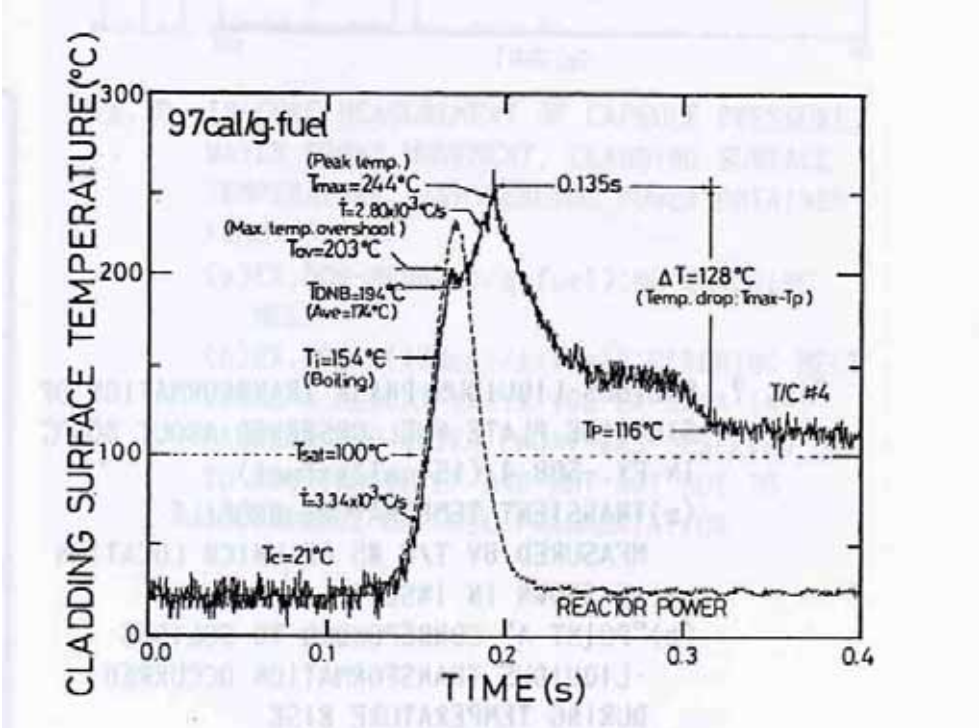

Figure 3: Typical example of cladding surface temperature （solid line）and reactor power （dotted line）, showing boiling temperature （T_i）, DNB temperature （T_{DNB}）, maximum overshoot temperature （T_{ov}）, peak cladding surface temperature （T_{max}）, quench temperature （T_p）, temperature drop（ΔT）, and time to quench （t_p）. These are from T/C #4 of the mini-plate fuel used in experiment 508-8 （97 cal/g・fuel plate, failure）.

Above T_{DNB}, the increase in CST terminated at temperature T_{max} （244 deg.C）. The CST was then quenched to temperature T_p （116 deg.C） during an interval of t_p （0.135s）. The magnitude of the temperature difference is given by $\Delta T=T_{max}-T_p$ and is denoted here as the "temperature drop（128 deg.C for this case）". Note that peak CSTs measured in the course of experiments are above T_{DNB} except one which is performed intentionally to have peak CST<T_{DNB}（Experiment 508-12, 32 cal/g・fuel plate, see Table 2）.

In two experiments 508-4 and 508-5, all peak CSTs further exceeded the melting point of Al cladding. **Figure 4** shows a typical transient temperature around melting point observed in the former. Measured melting point of the Al cladding was found to be 579±36 deg.C, an average from 10 T/C's. It was lower than that （640 deg.C） given by the binary phase diagram due to the fin effect of the T/C's [6].

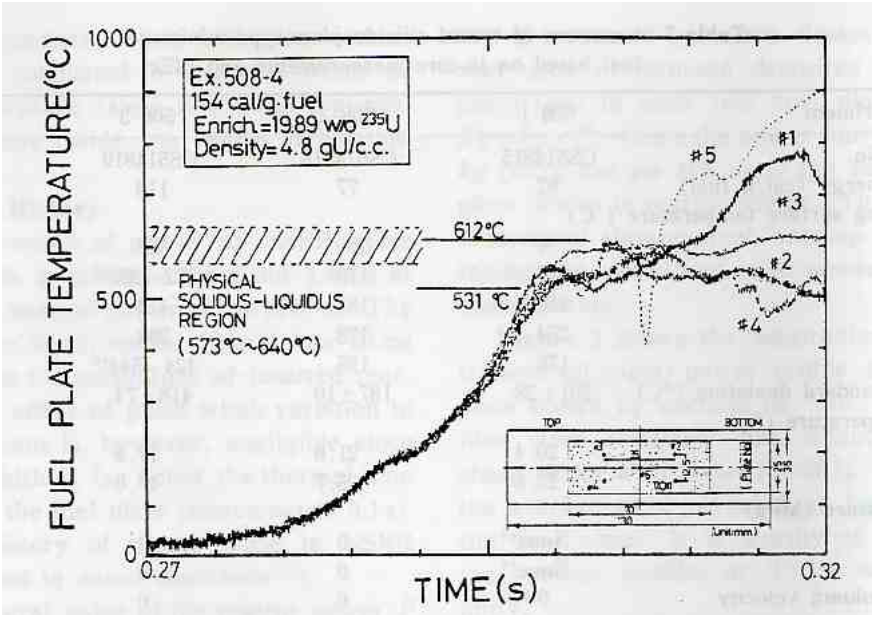

Figure4 Experimentally observed solidus-liquidus transformation temperatures of Al-3wt%Mg alloy （AG3NE）by T/C's welded directly to the mini-plate fuel surface, where physical solidus-liquidus transformation temperatures cited from binary phase diagram of the Al-3wt%Mg alloy are shown by hatched area for comparison.

3.2 Failure Threshold and Mechanism

Figure 5 summarizes the relation between the measured peak CST and the given deposited energy. Note again that all peak CSTs are above T_{DNB} except one case （32 cal/g・fuel plate）. The tested mini-plate fuel are intact at energy depositions <82 cal/g・fuel plate, while they are damaged at energy deposition >94 cal/g・fuel plate except one mini-plate pulsed at 98 cal/g・fuel plate without T/C's. The cause of this exception is not clear. The possible explanation is that the mini-plate having no T/C had rather uniformly quench because of no fin effect. The author consider from experimental facts that between 82 and 94 cal/g・fuel plate, a failure threshold must exist.

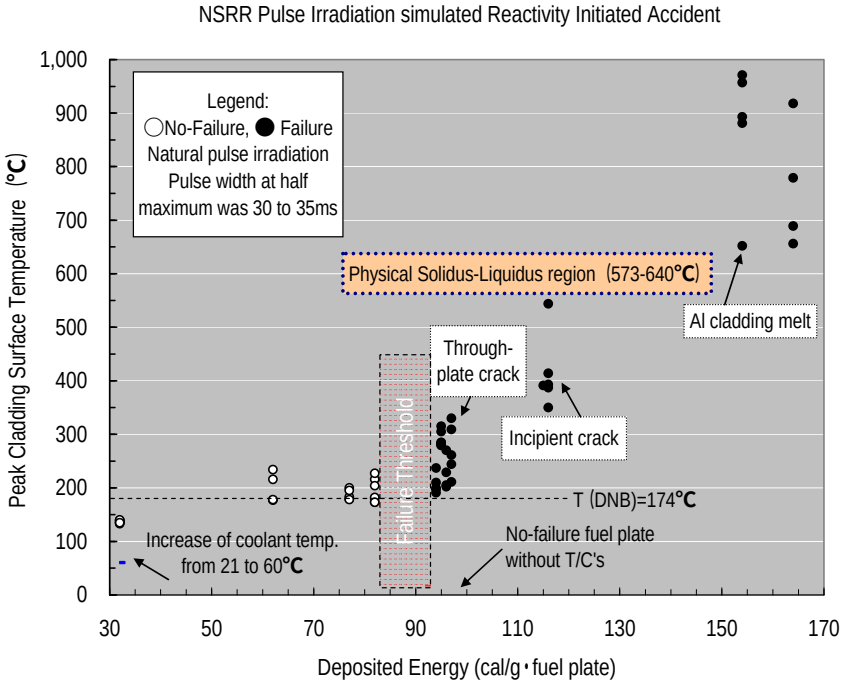

Figure 5: Peak cladding surface temperature read directly from the welded T/C as a function of deposited energy, where data point from experiment with no T/C is shown by arrow at the corresponded energy deposition. The dotted line indicates the T_{DNB} (174 deg.C)

The failure mode was dependent significantly on deposited energy, that is, CST. It is revealed from the figure that there are two failure modes. One is either a through-plate cracking (<400deg.C) or an incipient cracking occurred between 400deg.C and 640deg.C. The other is apparently Al cladding melt. Detail discussion about failure mode is as follows;

(1) Through-plate cracking failure

For through-plate cracking, a typical example is shown in **Photo 1** from B&W (94 cal/g・fuel plate, peak CST: 237deg.C). Two major through-plate cracks propagated perpendicularly from a cladding external surface to fuel core. These cracks are intergranular and rather tight, and they existed locally. This occurred without accompanying significant dimensional changes to the tested mini-plate fuel. The observed damage is likely to be a hardening crack led by a thermal stress due to the temperature drop ΔT. The calculated thermal stress caused by ΔT is ranged between 156MPa and 216MPa, which is greater than the tensile stress (120MPa) and 0.2% proof strength (85MPa) of B&W mini-plates. It implies that the local stress arising from the temperature drop ΔT during the quench is enough to affect on test mini-plate fuel cracking. On the other hand, the calculated thermal stress for CERCA fuel ranged between 175 and 394MPa, which is close to or greater than the tensile stress (230MPa) and the 0.2% proof strength (125MPa) of the CERCA mini-plate fuels.

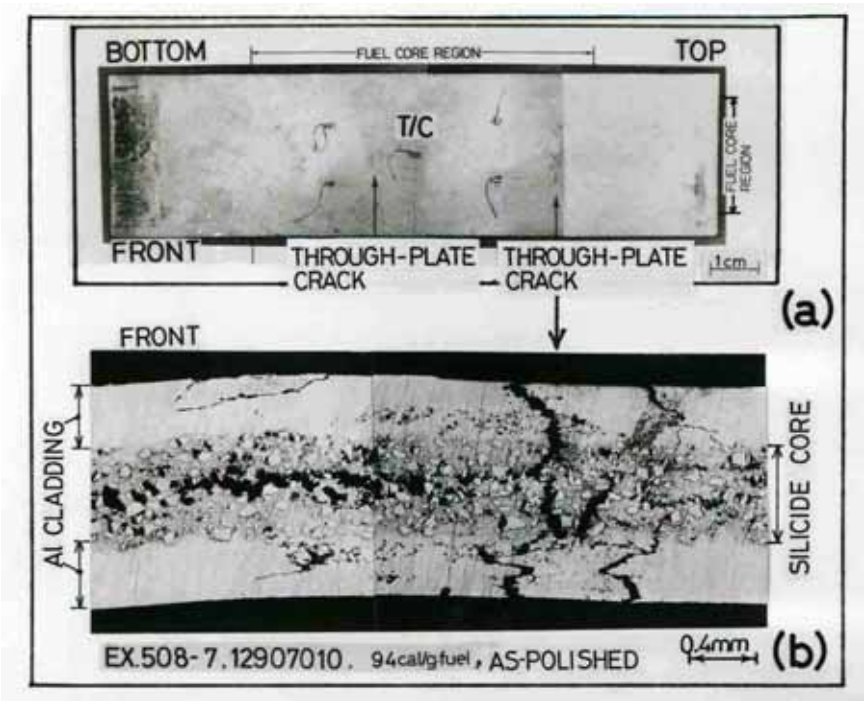

Photo 1: （a）Overview of the test mini-plate fuel at 94 cal/g・fuel plate （B&W, peak CST: 237 deg.C）, where two through-plate cracks occurred locally.（b）The polished longitudinal section cut from the through-plate crack at the plate top region.

(2) Incipient cracking failure

As shown in **Photo.2**, at temperatures between 400 and 640 deg.C, the test mini-plate fuels failed by incipient cracking, accompanied by a significant plate deformation. This seems to be due to annealing of Al cladding. Namely, crack propagation from Al cladding surface during quench might be ceased at annealed (softened) Al material.

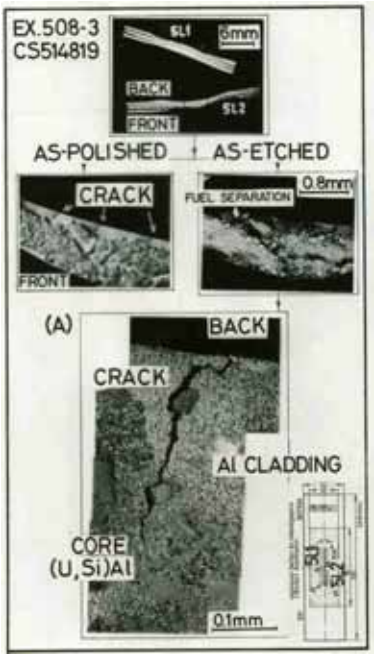

Photo2. Cross section of pulsed mini-plate fuel at energy deposition 116cal/g・fuel plate in experiment 508-3, where peak CST was about 544deg.C. Increase and decrease of meat thickness due to cladding melt is clearly observed.

(3) Al cladding melt

At temperature beyond the Al cladding melt, the test mini-plate fuel failed accompanied with significant formation of molten Al holes, molten Al agglomeration, fuel core separation, and through-plate cracking. This is shown representatively in **Photo 3 and Photo 4.**

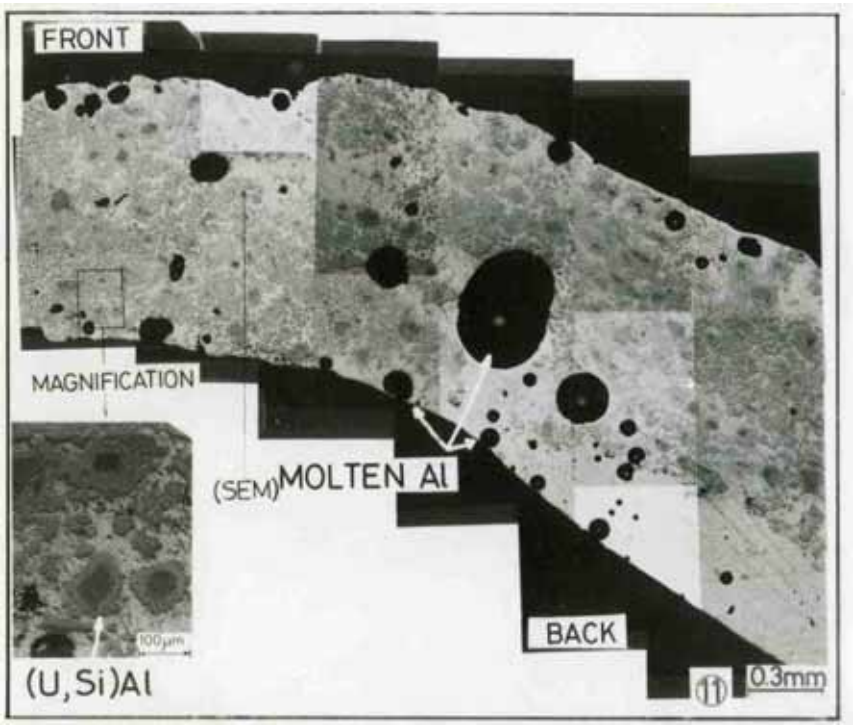

Photo 3: Cross section of pulsed mini-plate fuel at energy deposition 164 cal/g・fuel plate in experiment 508-5, where peak CST was about 918deg.C. Formation of molten Al holes and molten Al agglomeration is seen.

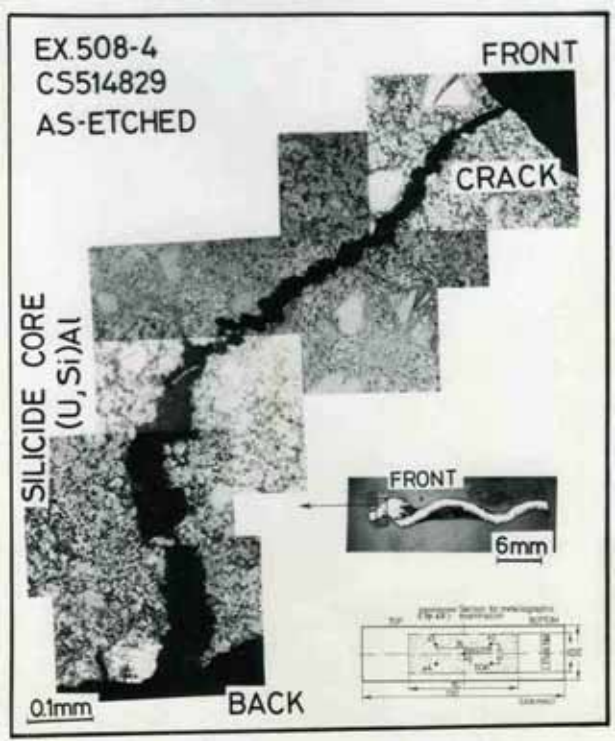

Photo 4: Cross section of pulsed mini-plate fuel at energy deposition 154 cal/g・fuel plate in experiment 508-4, where peak CST was about 957deg.C. Through-plate cracking and fuel core separation are seen.

In **Fig.6**, in-core data for no cladding melt condition and for cladding melt one are shown. In both cases, neither detectable increase of capsule pressure nor movement of water column was observed. Hence, in spite of drastic damage, the test mini-plate fuel did show neither fragmentation nor destructive force that would be expected from interaction of molten fuel with coolant.

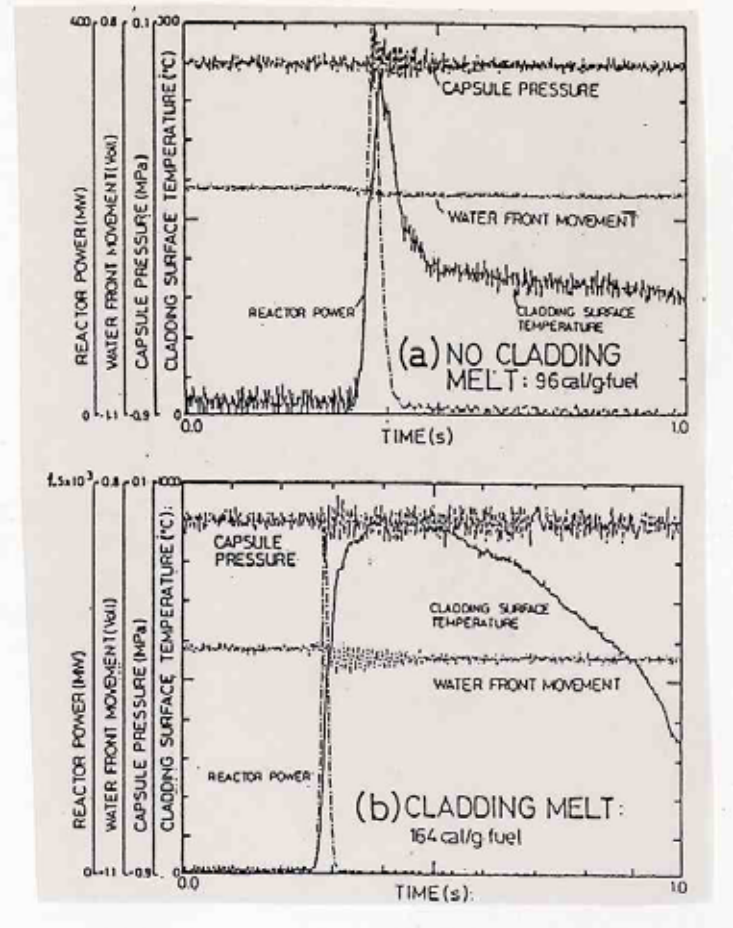

Figure 6: In-core measurement of capsule pressure, water front movement, cladding surface temperature and reactor power as a function of time. These are from （a）experiment 508-6 （96 cal/g・fuel plate, no cladding melt） and （b） experiment 508-5 （164 cal/g・fuel plate, cladding melt）. In the latter, a little variation immediately after pulse occurred at capsule pressure and water front movement due to a natural convection of coolant.

In **Photo 5**, SEM/XMA （scanning electron microscope combined with x-ray micro analyzer）photographs obtained from experiment 508-5（peak CST>746 deg.C） and that obtained from experiment 508-6 （peak CST<270 deg.C）are shown. In the latter, a microstructure composed of fuel elements U, Si and Al did not change significantly. In the former, however, a reaction between aluminium matrix and silicide particle did occur due to the diffusion of the composed elements. As a result, two additional new phases at outermost of the silicide particles were formed.

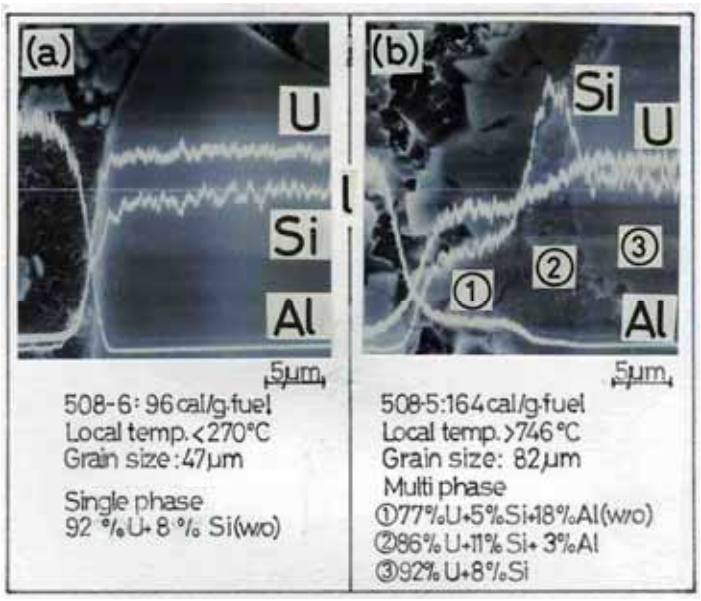

Photo 5: SEM/XMA examined along line *l* shown in the central part of the picture, where （a） specimen from experiment 508-6 （96 cal/g・fuel plate, peak CST<270 deg.C） and （b） specimen from experiment 508-5 （164 cal/g・fuel plate, peak CST>746 deg.C）.
A relative magnitude of detected elements was
Al : S_i :U =1 : 1: 5 for case（a）
and
Al : S_i :U =1 : 2.5: 5 for case（b）.

3.3 Dimensional Stability

JRR-3 safety analyses principally performed by the EUREKA-2 computer code predicted that the maximum PCST after water channel closure was about 228deg.C for silicide fuel. From the viewpoint of verification, a dimensional stability was studied by data obtained from PIE. Hence, the magnitude of bow, that is, the magnitude of water channel closure was determined by specimens cut longitudinally or transversally from pulsed mini-plate fuel. These data are also summarized in Table 2. During PIE, either longitudinal or transversal cut was made along to the T/C. Therefore, a dimensional stability of the plate could directly be related to the measured peak CST.

In **Fig.7**, a maximum bowing of the silicide mini-plate fuel is shown. Up to the mini-plate fuel temperature of 400deg.C, the bowing was less than 1mm（42% gap closure in maximum case), still remaining a safety margin for the coolant flow. When the temperature was exceeded 400deg.C, however, bowing became greater and closed the water gap. The magnitude pf bow was enhanced significantly by occurrence of necking, that is, a marked thinning of the plate wall thickness at the end peak locations. Such condition is shown in **Photo.6**. Strictly speaking, the magnitude of bow determined by a single plate configuration may not enough for discussing the safety margin of water channel closure because in conventional research reactor many fuel plates are assembled together. To simulate such multi-bundle condition, at least a pulse irradiation by triplet configuration is necessary. The author has done such kind of experiment. The results are another topics of a separated report.

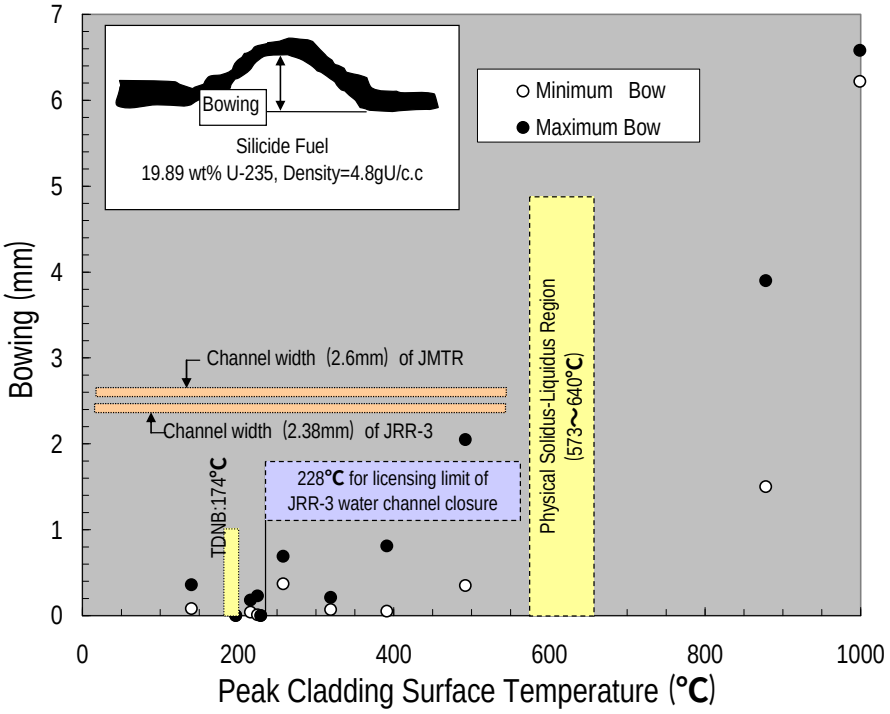

Figure 7: Observed maximum bowing of silicide mini-plate fuel at PIE, where cuttings a plate were made either of longitudinal （T/C #5） or of transversal sections （T/C's except #5） in order to contain at least one T/C in a cut specimen

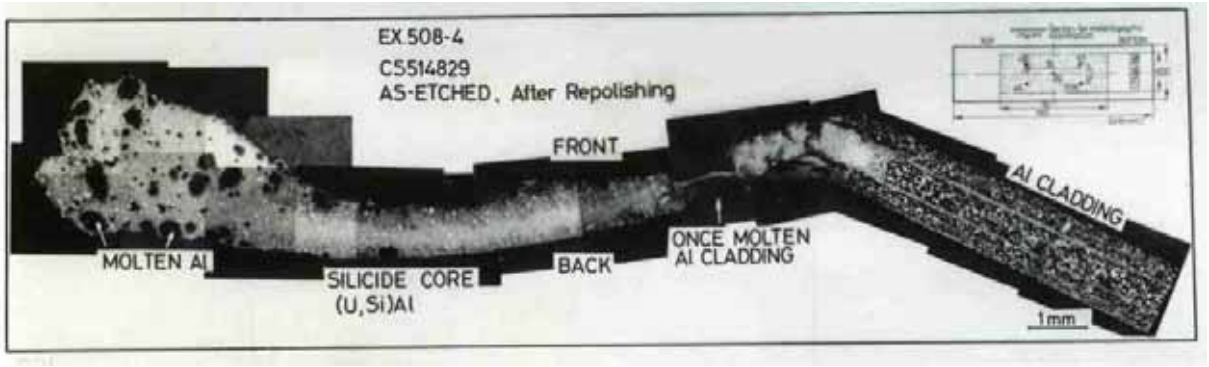

Photo.6 Cross section of pulsed mini-plate fuel at energy deposition 154 cal/g・fuel plate in experiment 508-4, where peak CST was about 957deg.C. The marked thinning of the plate wall thickness at the end peak locations (necking) occurred locally and enhanced the magnitude of plate bowing.

4 CONCLUSIONS

The conclusions reached in the present study are summarized as follows:

(1) The tested silicide mini-plate fuels were intact at energy depositions <82 cal/g・fuel plate but were damaged at energy deposition>94 cal/g・fuel plate. A failure threshold must exist between these two values. Departure from nucleate boiling about 174 deg.C and temperature drop ΔT>72 deg.C during quenching occurred in all tested fuel plated at energy deposition >62 cal/g・fuel plate.

(2) The failure mechanism was dependent on the energy deposition, in turn was strongly associated with the peak CST of the test fuel plate. Failure at temperature below 640deg.C （Al melting point）is caused by the thermal stress caused by the temperature drop during the quench. Several local intergranular cracks perpendicular to the axial direction of the plate have propagated from the cladding external surface to the fuel core. Test mini-plate under this situation showed little dimensional changes. Failure at temperature above 640deg.C is caused by the Al cladding melt. Test mini-plate under this situation showed large dimensional changes

(3) Below the temperature 400deg.C, the fuel plate bow was less than 1mm (42% channel closure in maximum), which remained the safety margin for coolant flow. When the temperature was exceeded 400deg.C, however, the fuel plate bow became greater and caused the closure of water gap. The bow was enhanced significantly by occurrence of necking, that is, a marked thinning of the plate wall thickness at the end peak locations.

(4) Within this experimental scope (temperature <970 deg.C）, no destructive force as a result of interaction between molten Al and coolant was observed.

REFERENCES

[1] F. YOSHINO and R. KIMURA; *JAERI-M 92-028,* (1992）, *Outline of Examination Guides of Water-Cooled Research Reactors.*

[2] USNRC; NUREG-1313, （1988）, *Safety Evaluation Report Related to the Evaluation of Low-Enriched Uranium Silicide-Aluminum Dispersion Fuel Use in Non-Power Reactors.*

[3] Y. FANJAS, *Proc. 3rd Asian Symposium on Research Reactor*, p.399 （1991）, *MTR fuel inspection at CERCA.*

[4] K. YANAGISAWA, T. FUJISHIRO, O. HORIKI. K. SOYAMA, H. ICHIKAWA and T.

KODAIRA, *J. Nucl. Sci., Technology*, 29 {3}, 233（1992）, *Dimensional stability of low enriched uranium silicide plate-type fuel for research reactors at transient conditions.*
[5] ASTM (American Standard for Testing and Materials): E 321-96(2005) *Standard test method for atom percent fission in Uranium and Plutonium fuel (Neodymium-148 method).*
[6] T. FUJISHIRO, *JAERI-M 84-063*（1984）, *A study on gap heat transfer of LWR fuel rods under reactivity initiated accident conditions.*

TOPSAFE
Dubrovnik, Croatia, 30.09 - 3.10.2008

Reevaluation Of BDBA Consequences Of Research Reactors

Guillaume BIAUT, Thierry BOURGOIS, Giovanni B. BRUNA

French Institute for Radiological Protection and Nuclear Safety

31, avenue de la Division Leclerc, 92260 Fontenay-aux-Roses, France

guillaume.biaut@irsn.f, thierry.bourgois@irsn.fr, giovanni.bruna@irsn.fr

ABSTRACT

Up to now, the French aluminium plate-type, water-moderated research reactors have been designed accounting for the consequences of a core disruptive RIA, assuming an envelope bounding thermal energy release of 135 MJ during the power transient, and a mechanical energy delivery in the thermodynamic interaction between molten aluminium and the liquid water of 9% of the whole thermal energy. According to the IRSN, both BORAX-I, SPERT-I destructive tests and SL-1 accident do not show restrictive phenomena on the thermal energy release, which mainly depends on reactivity insertion and core features. Consequently, in the framework of "Beyond Design Basis Accident" (BDBA) analysis, IRSN has decided to study scenarios representative of large reactivity insertion sequences using a semi-empirical simplified model and extending the application of the coupled neutronics-fluid dynamics code SIMMER, originally developed for LMFR, to the BDBA field in water-moderated research reactor. An innovative method to improve the treatment of resonance self-shielding in heterogeneous media has been developed; a model to treat fuel plate geometry has been implemented and new clad-to-coolant heat transfer coefficients suitable for extremely fast transient conditions, have been adopted. For the large reactivity insertion sequences tested, it was found that the geometry of the core immediate surroundings (including the narrow coolant channels and the reactor vessel, with a coolant inlet and coolant outlet separated from the main pool), has a major impact on the transients. The investigation of structure failure model can finally answer questions about the mechanical energy release, the deformation potential, the influence of failure on mechanical loads elsewhere, and the maximum local pressures.

1 ACCOUNTING OF RIA SEVERE ACCIDENT FOR FRENCH RESEARCH REACTORS

Core destructive tests carried out in the United States in BORAX-I reactor in 1954 and SPERT-I in 1962, as well as the accident which occurred on January 3, 1961 in SL-1 reactor in the United States (Idaho), have emphasized that water-moderated with aluminium-type fuel reactors could be, in case of a fast and large reactivity insertion, dramatically damaged by violent excursions of power involving degradation, even the fast melting of a part of the core, as well as the partial or total degradation of reactor structures of the. The thermal energy released generates a water steam bubble, by fuel-coolant interaction (FCI), which expands in the primary loop and in the reactor pool, with shock waves. This accident can particularly induce:

- the destruction of experimental devices, which can contain non condensable gas,

- the damage to the reactor pool walls,
- the weakening containment lower part, by thermal effects of not dispersed melted materials,
- a water spray to the hall of the reactor,
- a production of hydrogen by the oxidation of aluminium by the steam water,
- a damaging of the upper part of the containment (hall of the building), due to the increase of both temperature and pressure, and, maybe, a hydrogen explosion,
- the transfer of rare gases and volatile fission products to the hall of the reactor building, as well as a possible drive of fragments or fuel particles in this hall, etc.

In France, this type of accident, named BORAX, is taken into account in the design of research reactors. Although considered as a "Beyond Design Basis Accident" (BDBA), which induces strong arrangements to prevent its occurrence, this accident actually is an extension of the "Design Basis Accidents" (DBA) domain through design of important safety related equipments (containment buildings, walls of the pools, post-accidental heat removal systems, filtration devices, etc.); accordingly, these important equipments have functional requirements in order to allow mitigating the BORAX.

In the case of the French research reactors, this accident has been historically accounted for through an energetic approach. The main assumptions were, for all the reactors, a thermal energy of 135 MJ delivered in fuel during the transient of power and a mechanical energy, from the FCI as much as 9% of thermal energy. These assumptions have been adopted for the last research reactors built in France, namely the High-Flux Reactor in Grenoble and the reactor ORPHEE in the Saclay Nuclear Centre.

In 2003, during the assessment of the JHR (Jules Horowitz Reactor) safety options, IRSN wondered upon these *a-priori* assumptions, because several main features reduce the representativeness and the transposition of destructive tests such as BORAX-I, SPERT-I to the RJH case. IRSN mainly noticed that:

- the fuel of those reactors was high enriched in ^{235}U (93%), which is not the case for many current research reactors, and, in particular, the JHR;
- no absolute limit seem existing on the thermal energy release: this energy depends strongly on the introduced reactivity and kinetics. The three reports BORAX-I, SPERT-I and SL-1 do not provide any element likely to justify that the value of 135 MJ is an absolute maximum.

Consequently, IRSN considered that it was advisable adopting another approach for this type of accident, based on the study of scenarios representative of the sequences of reactivity introduction, to be taken into account in the BDBA scope, accounting for all available knowledge and adopting up-to-date modelling to study the phenomena brought into play. Following the request formulated in this direction by the French Safety Authority, the studies carried out by the CEA for the JHR preliminary safety report lead to a thermal energy in case of BORAX higher than 135 MJ. For the expertise needs, the IRSN undertook, in collaboration with various international partners and mainly FzK, an adaptation of the code SIMMER-III, originally designed for the fast reactors sodium-cooled. This paper displays some present aspects of this important work in progress.

2. SIMMER-III MODIFICATIONS FOR MODELLING RIA IN RESEARCH REACTORS

SIMMER consists of three modules: for space-time neutron kinetics, for reactor structures, and for multiphase multi-component transient compressible fluid dynamics. SIMMER is dedicated to LMFR Safety studies [1].

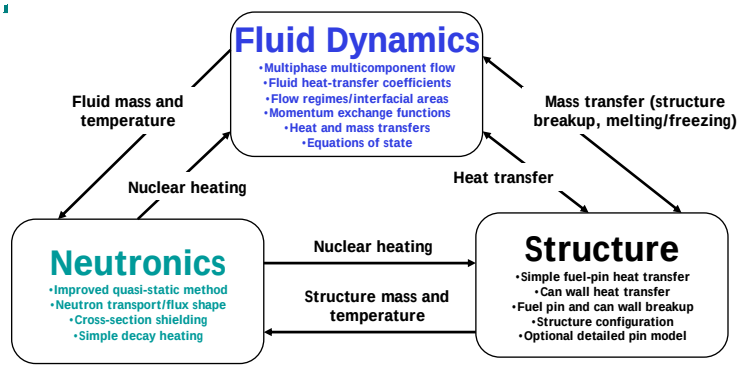

Figure 1**:** SIMMER overview

It is built on two superposed Eulerian meshes with cells that are consistent with the needs of both, the neutronics and fluid dynamics. For each of the eight major components, a full beyond-van-der-Waals equation of state is used [2], and each mobile component can have its own velocity.

1.1 Neutronics

The implementation of the neutronics part of the code has been carried-out with FZK, which has extended available and generated new cross section data libraries for SIMMER thermal reactor application. It has also improved the code with respect to neutron up-scattering and to the heterogeneity effect treatment in thermal reactors.

A set of codes for cross-section processing available at FZK has been extended in order to provide data in the JNC-extended CCCC format, and has been used for including data (from the ENDF 6.8 data library) for Be-9 (metal) in the 18-group library that is currently employed at IRSN for RHJ studies. Data for Be-9 are required for modelling of the research reactor reflector.

A new 40-group library for SIMMER that may be adopted in future studies on research reactor has also been implemented. Test calculations - performed by now at FZK - show that this 40-group data library provides more accurate results (compared to the 18-group one) for a set of thermal reactor models proposed by IRSN for benchmarking of SIMMER neutronics capabilities.

It has been extended the cross-section processing part of SIMMER in order to include a newly developed technique for taking into account heterogeneity effects. The preliminary results show that this technique improves the accuracy of calculations for the reactor models proposed by IRSN. Additional efforts on validation of the mentioned technique will probably be performed during this year

From the initial runs for simplified geometric arrangements it was obvious that the currently available version of SIMMER was not particularly well suited for the treatment of thermal reactors. Especially the neutron up-scattering during transients was not dealt with efficiently. As we already knew about this shortcoming from own experience, we were able to implement corresponding improvements fairly quickly which helped appreciably to improve the performance of the so-called gamma-iteration. Some unexpected difficulties with convergence performance, which may be related to rather coarse spatial meshes and correlated negative flux fix-ups had to be investigated in detail and suitable improvements have been implemented in an updated version of SIMMER. At present, it cannot be completely excluded that further modifications will be needed e.g. for a much more refined model of research reactor with smaller meshes and/or adoption of more energy groups.

1.2 Reactor structures

The description of the interior of the reactor structures can deal with undestructed geometry in which three characteristic temperatures are given in each cell in order to model heat conduction, a state of destruction inception where a part of the structures remains intact, and a fully destructed state where all liquid and solid debris move and interact with the liquid or gaseous coolant. Destruction inception is based on threshold temperatures, melted volume fractions, and/or pressures in the interior of the structures.

Rising fuel temperatures have two main effects: first, the Doppler broadening reduces reactivity, and second, the fuel dilatation reduces the presence of water next to the fuel thus lowering the level of neutron slowing-down. The water that is pushed out of a given cell flows to its neighbours. As will be described below, the fuel structure can exchange energy and momentum at its surface with the coolant water. SIMMER possesses a heat transfer correlation based upon transient overpower experiments in the NSRR reactor [3] with conditions very similar to those of the present study (see figure 2).

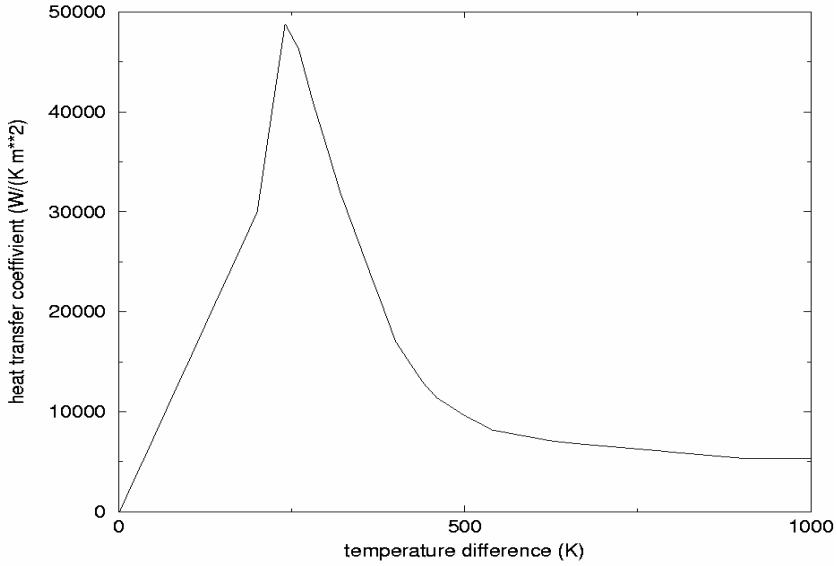

Figure 2**:** SIMMER heat transfer coefficient for transient boiling

Beside the fuel elements, the code describes the transient behaviour of left and right subassembly outer structures (in research reactor the casier) each of which having two characteristic temperatures. These structures can also melt or mechanically fail.

1.3 Fluid dynamics

The model describes the movement of continuous and discontinuous fluids including solid particles in a staggered Eulerian mesh with state values defined at the cell centres, and velocities at the cell boundaries. The solution of the conservation equations of all components and states is of second order in space and time. A predictor-corrector method guarantees a smooth incorporation of the two other modules with the objective of conserving mass, momentum, and energy. The interfaces between all mobile components and between them and the intact structures are interfacial areas which depend on space and time. These areas are calculated using a simplified convection equation with built on source terms based on correlations from the multiphase fluid literature. A several year long verification program of this code part has been performed at CEA [4].

In the research reactor, the fuel channels are very narrow. It would be prohibitive to model all 296 channels individually. Instead, one SIMMER ensemble of fuel element and adjacent channel represents several ten channels. During a very rapid heat-up of the fuel, the temperatures in the water may vary substantially, from close to evaporation at the fuel element surface to slightly heated up in the channel centre. Because the heat is predominantly flowing into narrow layer at the structure surface, this results in an early water evaporation which, in turn, reduces coolant densities and lowers reactivity. Therefore, the coolant channel has to be divided into four radial sub-channels. The thickness of the sub-channel next to the fuel is chosen so that results of very fast heat-up transients in the PATRICIA experiment are well represented (Bessiron, private communication).

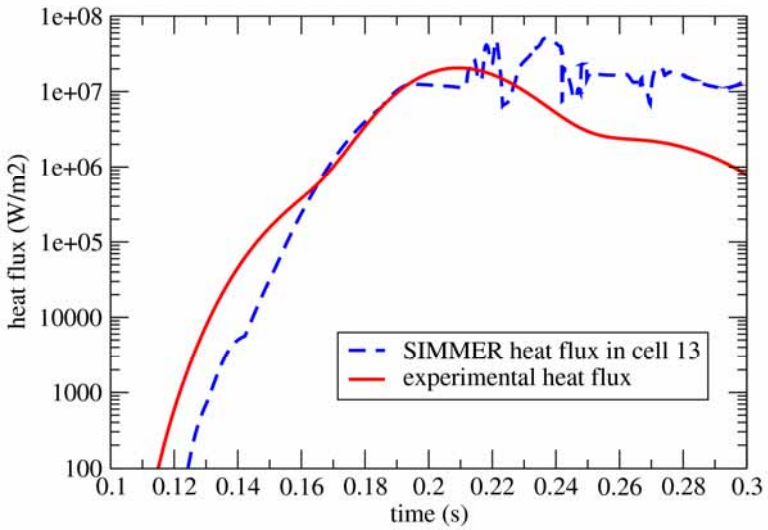

Figure 3: Comparison of PATRICIA results with a SIMMER calculation

Although second order solutions of the conservation equations can be adopted, numerical diffusion may extend over three adjacent fluid cells. The choice of four sub-channels is based upon the assumption that numerical diffusion and turbulent diffusion are of the same magnitude.

Upon destruction of fuel structures, liquid material and solid particles are injected into the coolant channel. The SIMMER calculations show that they penetrate to the farthest radial sub-channel. This is equivalent to the radial penetration of debris all over the research reactor channel. During a core-disruptive accident, fuel will fail first in the core centre, and then failure will propagate radially and axially to the core periphery. Under these conditions, the thermal interactions in the channels are first limited by the short penetration length. Water vapour is rapidly generated and superheated so that quite high pressures build up at the site of the first failure. Consequently, water is pushed out axially to the top and the bottom of the core. The kinetics of this movement is superposed to that of the propagation of fuel failure which advances in the same two directions. SIMMER can answer the question whether the voiding of the channels is slower or faster than destruction propagation, and whether the hot debris has a chance to efficiently interact with liquid water and thus increase pressures. The scenario of fuel coolant interaction has been verified for SIMMER [5].

In the SIMMER calculations, mechanical deformation beyond a representative channel cannot be taken into account. However, in research reactor, the radial deformation will be limited any way by the solid block of the casing.

The propagation of the pressure wave out of the narrow channels into the adjacent water plenum is limited by the sound velocity. Each code cell has a representative pressure. In case of propagation of the wave to the neighbour through a two-phase mixture, the derivative of density with the pressure is calculated. The derivatives of the mixture of components which is proportional to the mixture sound velocity are dependent on the local temperatures. The two-phase sound velocities are substantially lower than those of the single phase components, thus slowing down propagation.

At very high released thermal energies, the vapour may exit the core periphery and enter the water inlet and outlet plenum of the primary water cycle, which are carefully modelled by the code. Pressure drops are calculated using standard correlation for turbulent steady state flow. Orifice coefficients can be added to each cell. The perforated cylindrical flow distributor below the core is described by such coefficients.

While some structures outside the core may be rigid enough to withstand high pressures, others may fail early. In SIMMER, this is modelled by defining a threshold pressure at which the wall of the vessel is changed from a solid immobile structure to mobile particles. Although this may reduce inside-vessel pressures, the early part of the pressure waves may penetrate unmitigated to the bottom of the vessel.

Finally, the big vapour bubble enters the pool where it meets the bulk of cold water. At the bubble periphery, entrainment of cold water may take place. SIMMER has been verified on entrainment rates measured at FZK [6]. SIMMER also possesses the capability to take into account diffusion-limited condensation on the bubble surface in the case that non-condensable gases are present. This model has been verified on experiments performed at the Kyushu University, Japan [7]. Since the whole pool with its open surface to the ambient air is modelled, pool surface displacements and pressure loads are also results of the SIMMER calculations. The pool surface is influenced by two phenomena, first if the expanding vapour bubble is forced by structures to expand predominantly in axial direction an early doming of the surface becomes visible. Second, during bubble condensation, water of the upper pool starts to move downwards. This initiates a surface wave that can lead to increased doming if the wave is reflected at the pool wall and moves backwards to the centre of the pool.

2 RESULTS OF THE STUDY

Figure 4 outlines the research reactor geometry in SIMMER format, where the numbers at the side denote the axial and radial cell numbers.

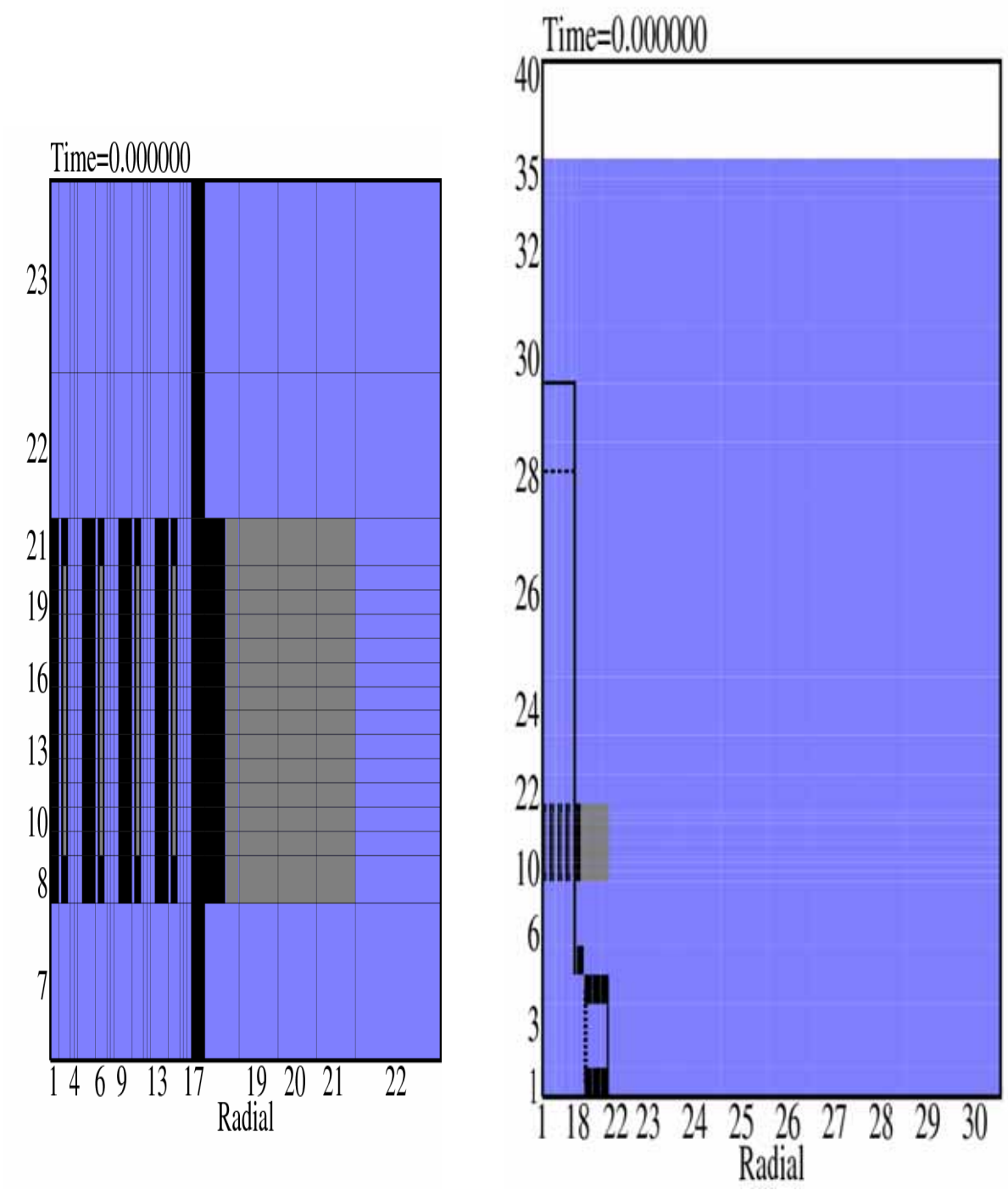

Figure 4: SIMMER core model

In the left part is shown the cylindrical core model of research reactor with reflector (grey), in the right the closed cylindrical vessel model of research reactor, dashed lines = perforated structures with orifice pressure drop, inside the reactor pool with an open water surface. The measures in the vicinity of the core were read from copies of artist's views of the

design. Axial and radial scales were not always consistent. The SIMMER geometry should be checked in the future. Two calculations are presented:

- a core within an indestructible vessel where the vessel lid has been removed (open vessel),
- a core within a detailed vessel including in-vessel perforated structures and a closed lid, where those axial parts than consist only of an aluminium wall of about 20 mm fail when the adjacent pressure exceeds a threshold value (closed vessel).

Both cases are calculated assuming a zero water velocity through the core. The initial pressure inside the closed vessel is about the same as outside. The transient starts before a steady state hydrostatic head inside and outside the vessel can be established. Therefore, pressure oscillations are still present when the core starts to be destructed. In a final study, a SIMMER pre-run with steady state power needs to be made until the hydrostatic equilibrium has been reached. The final state of this run will be used as the initial condition of the transient run. The closed vessel case has a threshold pressure of 11 bar. This value is probably below the failure pressure of the wall but it produces early vessel failure, and thus a reduction especially of pressure below the core. The following figure 5 shows the integral energetic results of both cases.

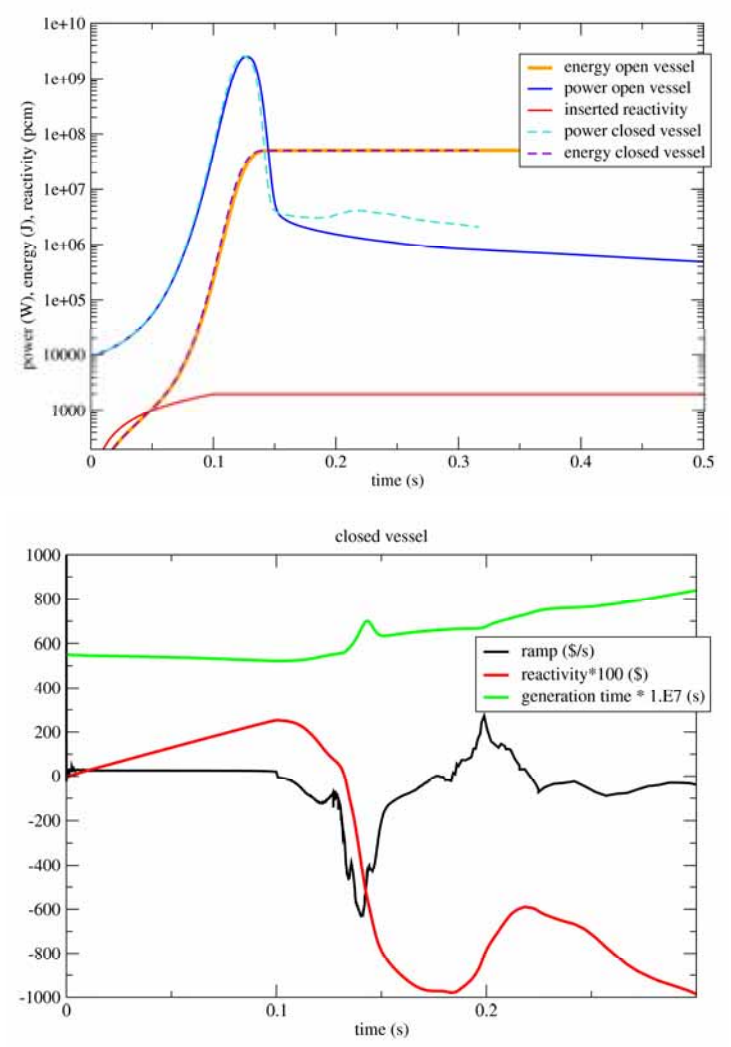

Figure 5: Comparison of PATRICIA results with a SIMMER calculation

They show little difference. The power in the case of an open vessel increases a very little bit later. The lower red curve represents the reactivity inserted (an input for the code). It is a linear ramp from zero to 2000 pcm at 100 ms. While the reactivity increases linearly until 100 ms, feedback become important afterwards. At 130 ms, the core starts melting, but the Doppler broadening and the moderation effects have already decreased the reactivity to close the initial value. Core destruction runs out at 160 ms. First the fuel temperatures rise, but the Doppler becomes effective only at higher values. Then water is leaving the core region pushed out by fuel dilatation which is also effective only a substantial temperature increase. Finally, as a consequence of FCI, the water vapour mass increases at the time the power is already down to half the peak value. A detailed picture of the core destruction is shown in the following figure 6.

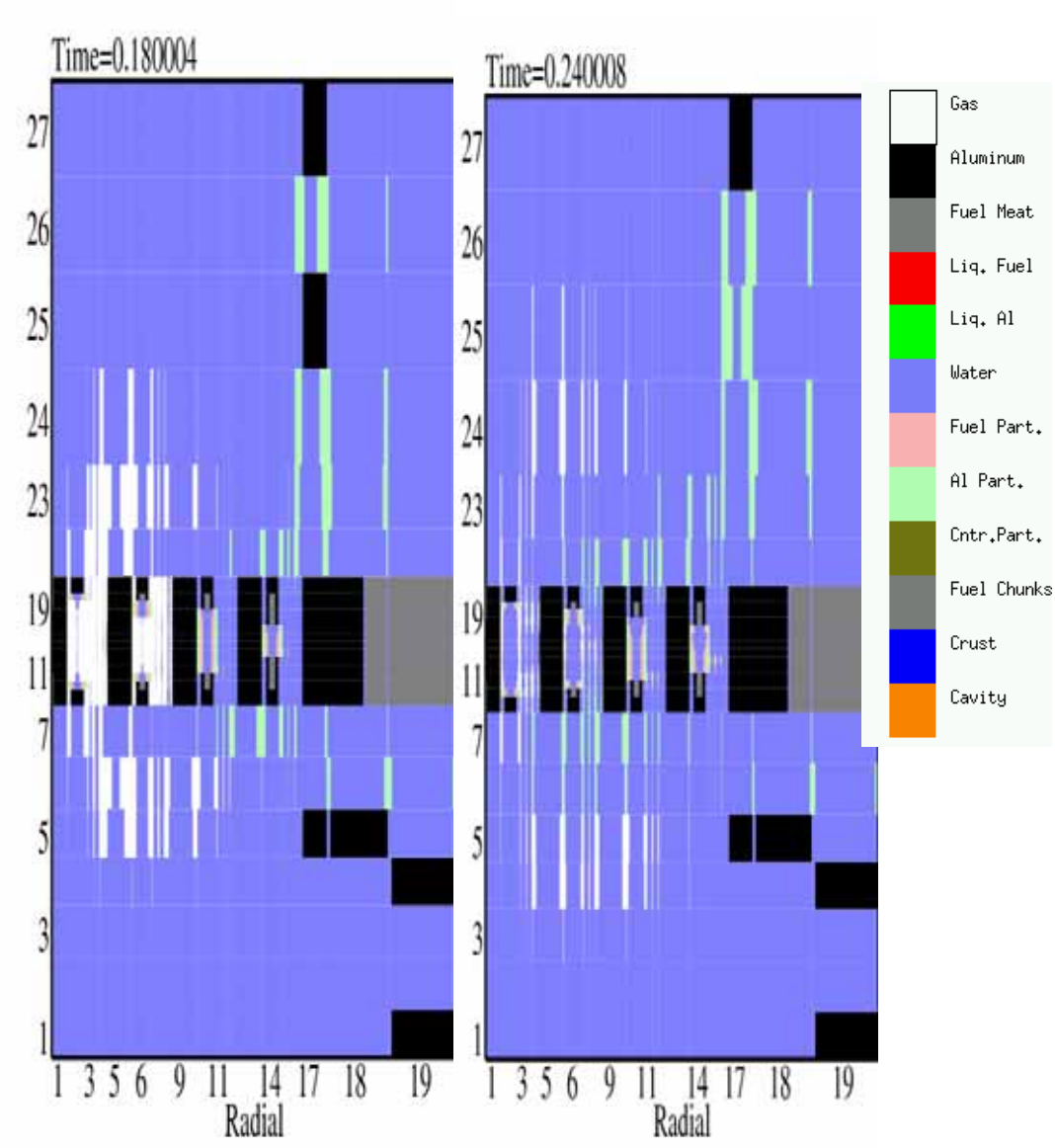

Figure 6: Side views of destroyed core

At 180 ms (left figure), the vapour bubble has reached its maximum size and starts to re-condense. Core destruction has progressed only little coming to an end at this time. At 240 ms (right figure), the vapour bubble has almost completely collapsed, and the core debris is cooled down effectively by the water.

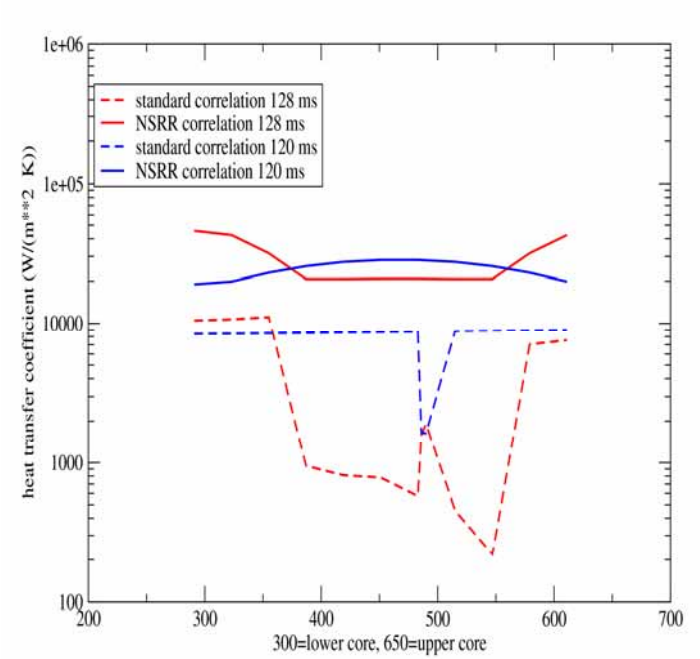

Figure 7: Fuel plates heat transfer coefficients (standard and NSSR)

Figure 7 shows that just before the fuel failure, which happens at 130 ms, the heat transfer coefficients of SIMMER-research reactor are significantly higher than those of standard correlations, which depend on fluid velocities. There is a negligible fraction of water vapour in the channel until the fuel plates fail and the subsequent FCI rapidly evaporates the water in the channel. Because the peak pressures are generated by FCI, it is important to study the condition under which FCI occurs. First, as already mentioned in the description of the code, the movement of hot debris from the fuel plates into the water channel is limited by the channel width. Then the generated vapour escapes axially upwards and downwards. In the following figure 8, the kinetics of this process will be demonstrated.

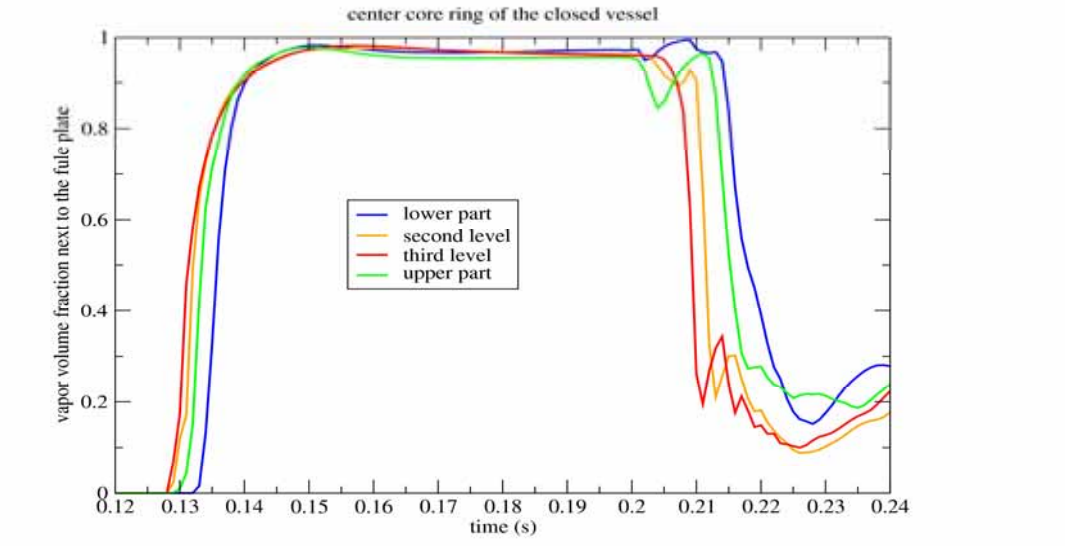

Figure 8: Vapour volume fraction close to the fuel plate

Figure 8 above here shows the volume fractions of the cells with fuel plates of centre core ring. It takes about 5 ms to void all cells of the core containing fuel plates.

Whether the voiding of the channels can influence local interaction must be studied by looking at two different radial cuts of the centre fuel ring of the core.

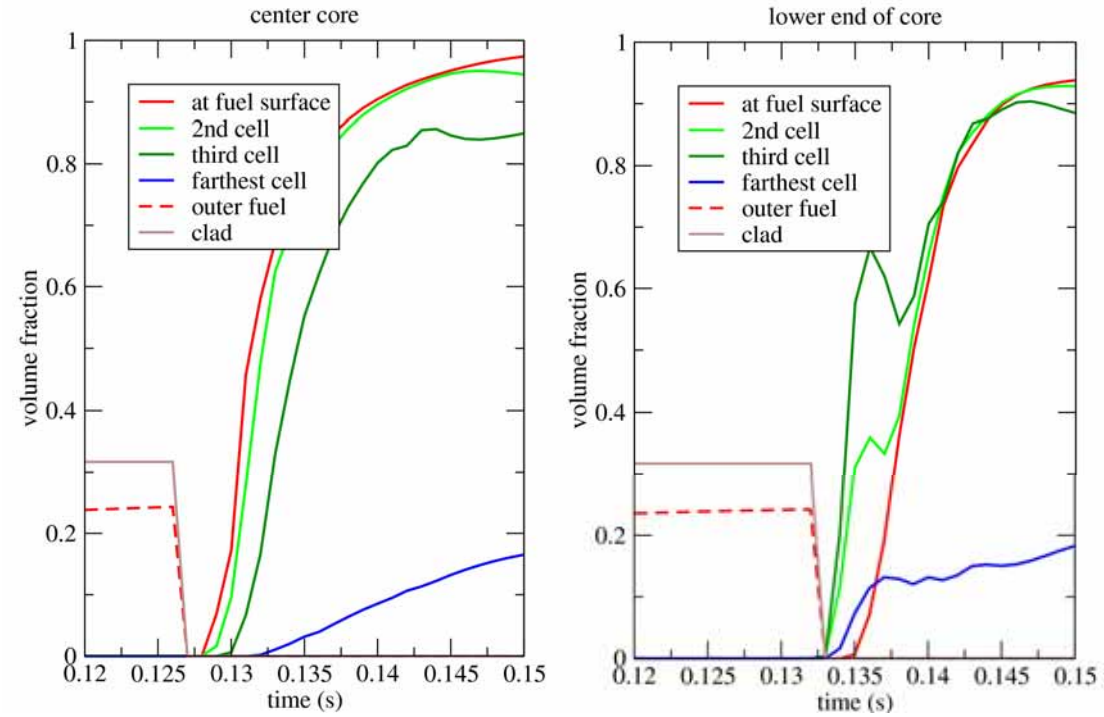

Figure 9: Vapour volume fractions

The figure 9 shows the volume fractions of the first two cells in the fuel plate and the volume fraction of water vapour. For the axial core centre, the four water rings adjacent to the fuel show voiding only 1 ms to 2 ms later than the simultaneous disruption of outer fuel and clad at 126 ms. This indicates that the debris are injected into a channel filled with water. For the right figure of the lower end of the core, there is less a time lag between disruption and voiding. The void profiles for the second and third cell show an earlier voiding than that of the cell of the fuel surface indicating that the bubble movement is predominantly in the channel centre.

To conclude, it is probable that the emerging bubble does not affect the efficiency of FCI in the core centre, but at its axial peripheries, the early presence of the bubble should decrease FCI.

The description above has enabled understanding the mechanisms that drive the pressures in the channels and outside of the core. The results show substantial difference between the open and the closed vessel. We need to keep in mind that the closed vessel is subjected to an early vessel failure below the core which results in a sort of open vessel. Simplifying the pressure-relevant conditions, the closed vessel is actually a vessel open below the core, and the open vessel is a vessel open above the core.

The figure 10 shows a comparison between pressure of the closed and open vessel cases. It demonstrates the time scales of the oscillations after peak power.

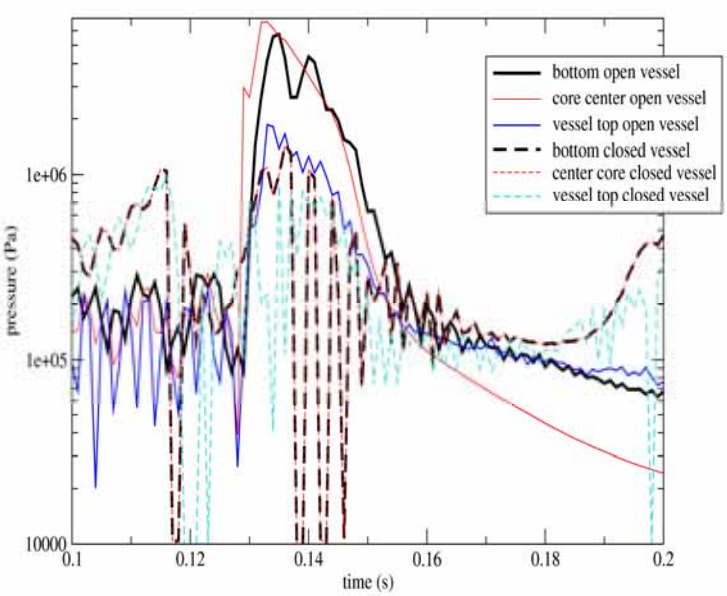

Figure 10: Open and close vessel pressure oscillations

The figure 10 shows in black the bottom pressures adjacent to the lower vessel wall which is of specific interest because its failure may lead to leakage. For the open pool at the maximum pressure, the radial distribution of this pressure is shown in the figure at the right. The value of the closed vessel is lower because of early vessel failure below the core. It shows high frequency oscillations. The maximum bottom pressure of the open vessel is 14 bar, that of the open vessel 57 bar. Oscillations prior to 120 ms are due to a start of the transient from a non-steady state of hydrodynamics.

To demonstrate the long time behaviour of the open vessel, the following figure 11 shows the vapour bubble (yellow) emerging from the core centre. It moves out of the core in both the upward and downward direction. Because the lower plenum is closed, the lower bubble does not penetrate further while he upper rises until almost half of the upper plenum is voided. Water displacement out of the upper plenum increases the pool surface (yellow).

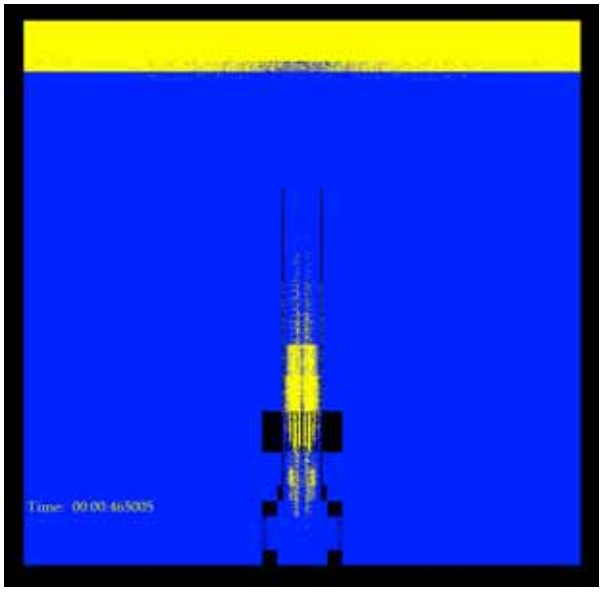

Figure 11

3 CONCLUSION

The coupled neutronics-fluid dynamics code SIMMER has been up-graded to treat Design Basis Accidents in experimental reactors with thermal spectra. The research reactor has fuel plates and water cooling channels of millimetre-size, so that effects of core heterogeneity on neutron flux distribution are smaller compared to conventional LWRs. Due to off-the-shelf SIMMER models, this allows defining fluid dynamics and neutronics computational meshes convenient to the specific needs. The code was improved including models which increase its representativeness. However, further validation of neutronics and fluid dynamics models adopted is still necessary and is underway. The objective of the improvements is to calculating the different reactivity feedbacks, the deposited thermal energy, and the sequence of core disruption, transfer of thermal to mechanical energy, and finally pressures at sensitive locations.

It was found that the geometry of the region surrounding the core has a dominant influence on the transient. The structure failure model can finally answer questions about mechanical energy releases, deformation potential, the influence of failure on mechanical loads elsewhere, and maximum local pressures.

REFERENCES

[1] Tobita, Kondo, Yamano, Morita, Maschek, Coste and Cadiou - The Development of SIMMER-III, An Advanced Computer Program for LMFR Safety Analysis, and Its Application to Sodium Experiments, Nuclear Technology, 153 [3], 245, 2006

[2] Morita, Fischer - Thermodynamic properties and equation of state for fast reactor safety analysis, Part 1: analytical equation of state, Nuclear Engineering and Design 183 (1998) 177-191), and each mobile component can have its own velocity

[3] Bessiron, Sugiyama, Fuketa - Clad-to-Coolant Heat Transfer in NSRR Experiments, Journal of NUCLEAR SCIENCE and TECHNOLOGY, Vol. 44, No. 5, p. 1–10 (2007)

[4] Wilhelm - Assessment of SIMMER-III Performance on Pool and Depressurization Experiments, STR/LML/95-315, Mai 1995

[5] Morita, Kondo, Tobita, Brear - SIMMER-III Applications to Fuel-Coolant Interactions, Nuclear Engineering and Design, Vol.189, pp.337-357, 1999

[6] Meyer, Wilhelm - Investigation of the Fluid Dynamics of a Gas Jet Expansion in a Liquid Pool, Forschungszentrum Karlsruhe report KfK 5307, March 1994

[7] Morita et al. - Development of multi-component vaporization/condensation model for a reactor safety analysis code SIMMER-III, Theoretical modelling and basic verification, Nuclear Engineering and Design 220 (2003) 224–239)F. M. LAST, The Title of the Book, page or chapter numbers, Publisher, City (year).

TOPSAFE
Dubrovnik, Croatia, 30.09 - 3.10.2008

Simulating a Partial LOCA in a Narrow Channel Using the DSNP Simulation System[1]

David Saphier
Soreq Nuclear Research Centre, Yavne 81800, Israel;
saphier1@013.net.il;
Present Address: 21 Netiv Halamedhe, Rehovot 76223, Israel
Tel +97289451743, Fax +97289491233

ABSTRACT

A partial LOCA accident in a pool type research reactor was investigated. A new MTR type fuel channel model for the DSNP simulation system was developed, permitting the calculation of detailed axial and radial temperature distributions. New and older heat transfer correlations were incorporated in the model. Simulations of accidental water levels of 14 and 35 cm during a partial LOCA in a 62cm narrow fuel channel were performed. The resulting maximum temperatures remain significantly below the aluminium melting point, and no damage to the core will take place under these conditions.

1 INTRODUCTION

A partial LOCA (Loss of Coolant Accident) is an extremely rare event in a research reactor. The purpose of this study was to investigate the consequences to the MTR type fuelled core having very narrow coolant channels, when the water level in a pool type research reactor remains at a level of between 20 to 55% above the fuel channel entrance. The water level is reduced due to a hypothetical guillotine break in either the primary coolant loop or in an experimental beam tube. A schematic description of the IAEA generic pool type research[4] reactor is shown in Fig. 1, emphasizing the location of possible pipe breaks which may cause a partial LOCA event. The reactor structure includes an open concrete cavity filled with demineralised water up to a level of 10m above the pool bottom. The core is placed on a grid plate located 1m above the pool bottom. Six to eight beam tubes can penetrate the pool concrete wall reaching the core edge and providing neutron beams for experiments.

Following power shut-down, upon the detection of the water leak through the severed pipe, the decay heat remaining in the core will heat-up the fuel, and water boiling in the narrow channels might take place. The boiling process, depending on the residual power level, will force some of the water out of the channel, and the boiling process may be considered as boiling under very low Reynolds number or some kind of pool boiling or percolation condition.

A model for these conditions was developed for the DSNP[1] (Dynamic Simulator for Nuclear Power-plants) system using a recently proposed heat transfer correlation by Zhang, Hibiki and Mishima[2] for small diameter channels, and several older correlations given partly

[1] Pap-262b, Topsafe-2008; Dubrovnik Croatia.

in Ref. [3]. The model was applied to study the behaviour of the IAEA generic research reactor[4] under partial LOCA conditions. This reactor is a pool type, light water, 10MW reactor, schematically presented in Fig. 1, using MTR type fuel elements. It is shown in the present study, that if the water level remains at or above 20% of the fuel channel length, that is, a partial rather than a full LOCA condition, no damage to the core will occur. This was also shown by the experiments performed at Livermore[5] and reproduced in this study.

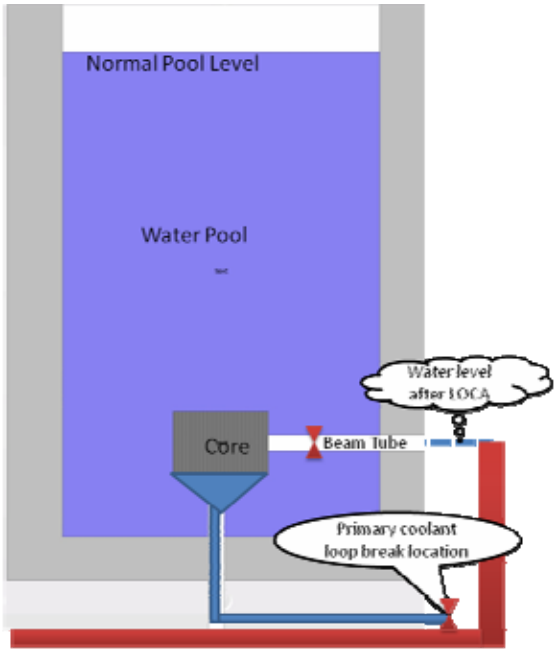

Fig. 1: Schematic drawing of an open pool type research reactor

2 THE LOCA ACCIDENT

The accident starts with a reactor operating at full power. In the case of a major break in one of the pipes, the water level in the pool starts decreasing. The reactor safety system will scram the reactor and further decrease in the water level will also stop the pumps. With no forced circulation a shutter valve will be opened by gravitational force and natural circulation through the core will be established removing the decay heat. Further decrease in the water level will eventually uncover the core and natural circulation ceases. The water in the core will start heating up and boiling will occur. A stable condition is achieved once the water level reaches equilibrium condition with the surrounding structures at some level along the core height. Most research reactors of this type are designed for the water level to stabilize at about mid-core or above.

A guillotine break in the primary loop or in a beam tube is modelled by starting an outflow of water from the pool via the broken pipe. The flow rate is determined by solving the momentum balance equations using the appropriate DSNP[1] models. The pumps are stopped after a short time, and the reactor is shut down. The power decreases rapidly until it reaches the decay heat level as shown in Fig. 2. The decay heat is calculated from the ANS standard curves for ^{235}U. Calculations have shown, that it will take about 21 min for the water flow to reach equilibrium conditions, as can be seen in Fig. 3, and the out-flow is reduced to zero. When the water reaches its equilibrium level, about mid core (according to the exact reactor and its surrounding geometric design features), this part of the simulation is terminated.

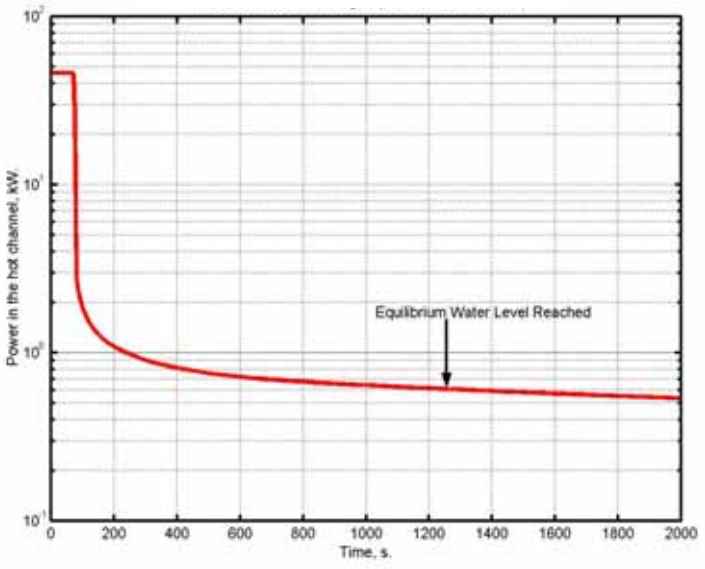

Figure 2: Hot channel power reduction during a partial LOCA accident

As can be seen from the above figures, the power at time of reaching equilibrium conditions in the hot channel is 600W and the water out-flow ceases at this time. The simulation of the core condition is stopped at this point and the prevailing conditions serve as input to the next step of simulating the hot channel under partial LOCA conditions with the water level at mid core.

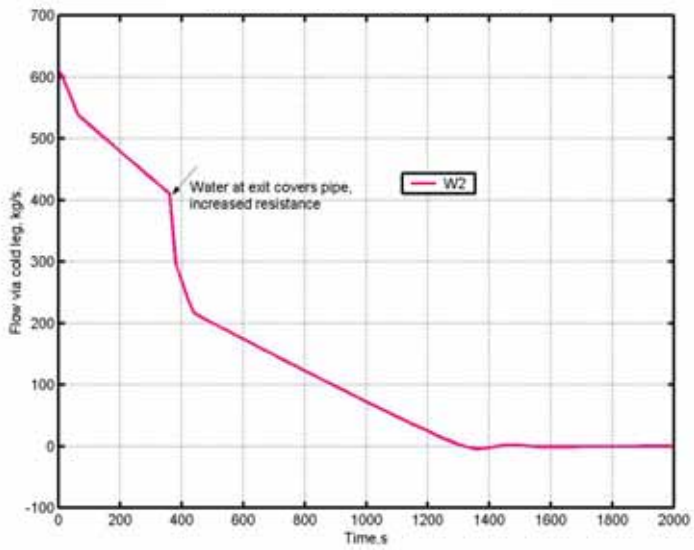

Figure 3: Water flow rate from the reactor pool following a break in the main coolant loop.

3 RESULTS OF THE SIMULATIONS

The results are presented here for a partial LOCA in which the equilibrium water level reached the mid-core level. Actually a level of 35cm from the coolant channel entrance was chosen (mid-core + 4cm), which is the equilibrium level following the LOCA event in the main coolant loop, for the geometry selected as shown in Fig. 1. In addition the low 20% core water level condition is also simulated in order to compare the results with the Livermore experiments[5]. All the results presented in this chapter are based on the simulations performed with the DSNP models presented in the next chapter of this paper. In Fig. 4 the power distribution in the hot channel and the actual power transmitted to the coolant are presented at the time when the equilibrium water level in the reactor pool is reached. The difference in the two distributions results partly from the changing heat transfer correlations due to the changes in the flow regime, and partly due to axial conduction of the heat along the fuel and the side plate. As can be observed part of the heat from the hot upper part of the fuel is conducted to the lower colder part of the fuel and the side plate. This can be concluded from the observation, that in the fuel plate lower part, more heat is transmitted to the coolant than the heat produced in this region.

Figure 5 shows the axial temperature distribution in the core hot channel in the fuel, the side plate, and the coolant channel. As can be seen the coolant enters the channel at 30^{o}C, and starts boiling at about 18cm. The water coolant mixture flows up the channel cooling it as it flows with the steam fraction increasing continuously but remaining at saturation temperature until exiting the channel. The flow characteristic changes along the channel, however the most appropriate description will be a dispersed film boiling or slug flow. The maximum metal temperature is 135^{o}C, which is significantly below the softening temperature of Al - about 400^{o}C. Fig. 6 shows the steam and water enthalpies along the channel. The steam and

water flow rates are shown in Fig 7. At this stage both the water and steam are still at saturation conditions. The water enters the channel at 30°C, and starts boiling at 18cm. It continues to boil along the channel and exits with a quality of 57%. Under more realistic conditions slugs of water will be moved up the channel, some of the water is expelled from the channel while part might flow back into the channel.

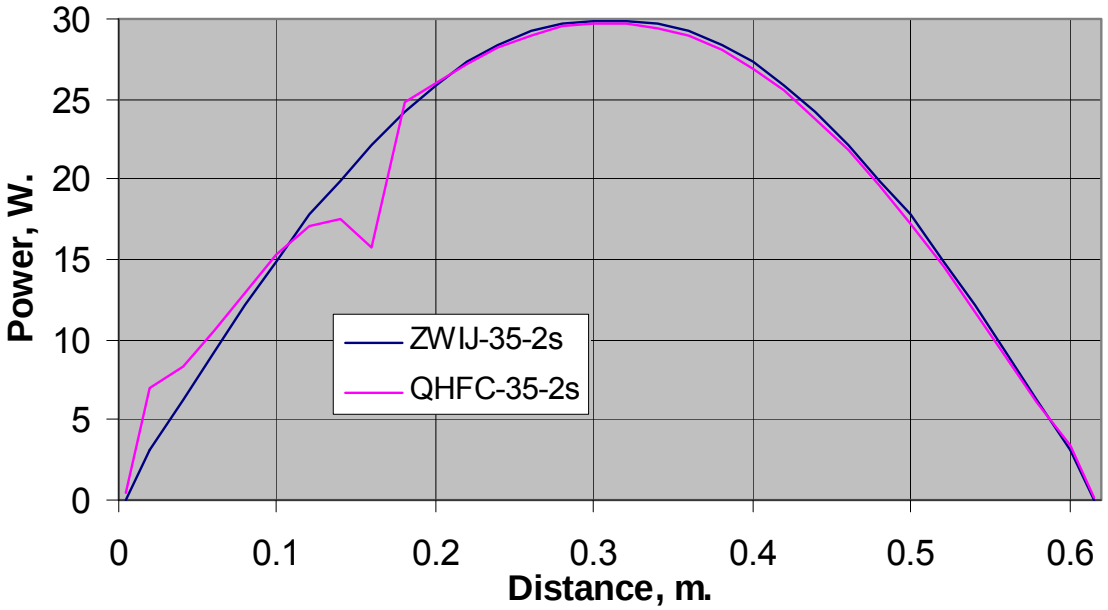

Figure 4: Power distribution along the hot channel (ZWIJ) and the power transmitted to the coolant (QHFC) at time of equilibrium water level conditions.

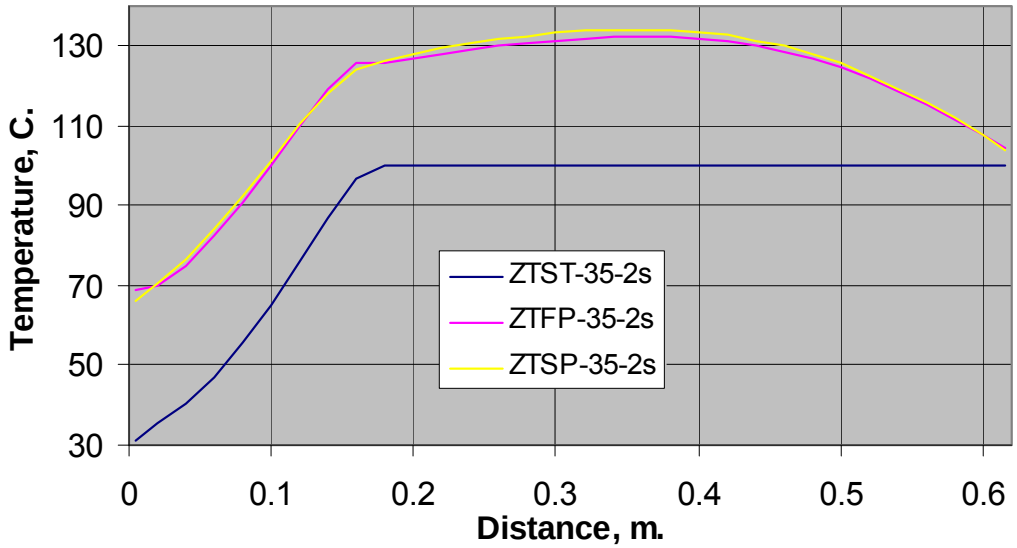

Figure 5: Fuel (ZTFP), side plate (ZTSP) and water-steam (ZTST) temperatures during a partial LOCA in the IAEA generic research reactor, equilibrium water level is at 35cm above the channel entrance.

Fig. 8, shows the axial temperature distributions for the case in which only 14cm of the core remains under water. This level was artificially chosen in order to compare the results with an experiment presented in Ref. [5] for the Livermore MTR fuel experiment. The distribution is presented using two different heat transfer correlations[3]. As can be seen the fuel temperatures are much higher than in the previous case reaching 270°C and 310°C, and the steam gets superheated in this channel.

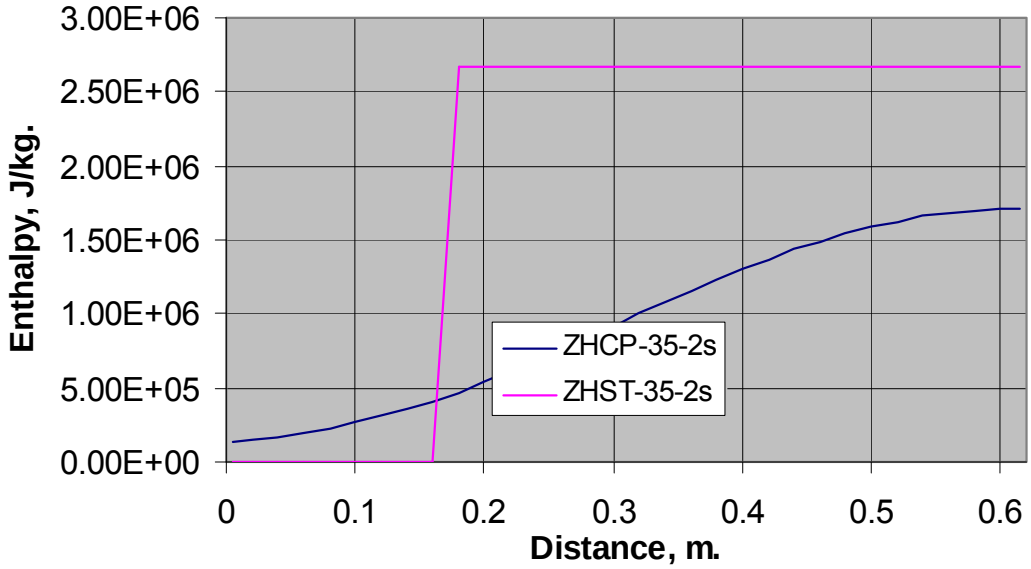

Figure 6: Water (ZHCP) and steam (ZHST) enthalpies along the coolant channel following a partial LOCA condition.

Some experiments with mock-up fuel channels performed at the Paul Scherer Institute[8], indicate that higher temperatures might result with the pool water level at 25cm. These results were not reproduced in the present study, and further theoretical and experimental investigations are underway for different pool water elevation, and different power ratings.

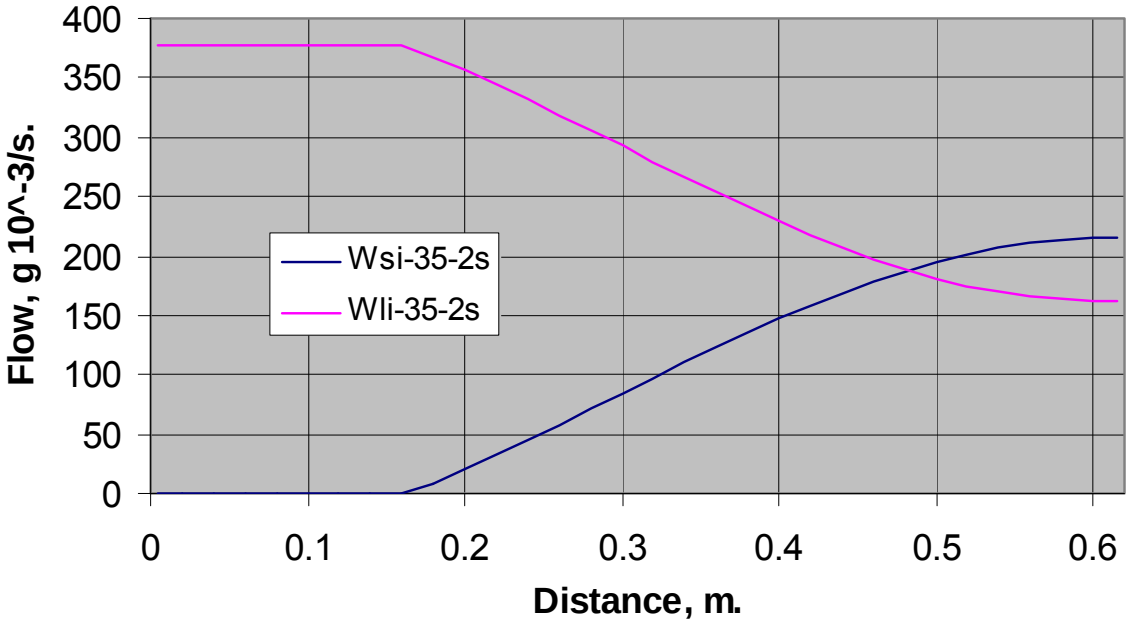

Figure 7: Water (Wli) and steam (Wsi) flow rates along the hot fuel channel, following a partial LOCA with equilibrium water level at mid-core.

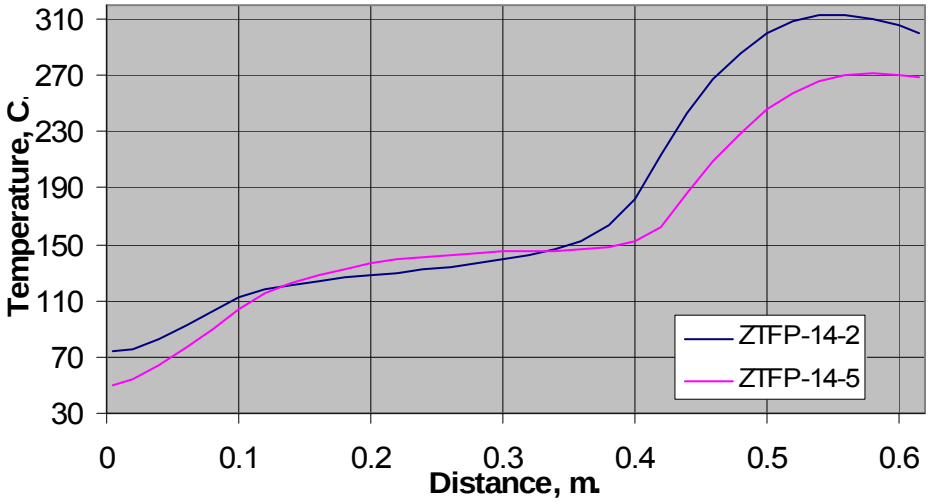

Fig 8: Fuel temperatures distributions with two different heat transfer correlations during a partial LOCA in the IAEA generic research reactor. ZTFP-14-2 htc from ref-3 and ZTFP-14-5 htc from ref-2. Equilibrium water level is 14cm above the channel entrance.

4 THE FUEL CHANNEL MODEL

In the literature there is very little information on boiling and dry-out in parallel channels of the MTR type fuel elements, as boiling in this type of research reactor is not expected. The closest model representing these conditions was developed by Hochreiter[9], and is presented below in Fig. 9. This model shows the fuel channel rewetting after dry-out with a very low flow rate entering the channel. The model was actually developed for high pressure conditions, while in the present case atmospheric pressure prevails.

The transition between the single phase liquid and the DFFB – Dispersed Flow Film Boiling condition is very rapid as even a small amount of steam requires a volume 1600 times larger than the liquid. At high pressure, for example 40 bar, this ratio is only about 40. Consequently one expects rapid creation of large bubbles pushing droplets or slugs of water in the upward direction, may be even out of the channel. This phenomenon was designated as “Percolation” in the Livermore SAR from 1974[5]. However, this phenomenon was not indicated or modelled in any subsequent publications.

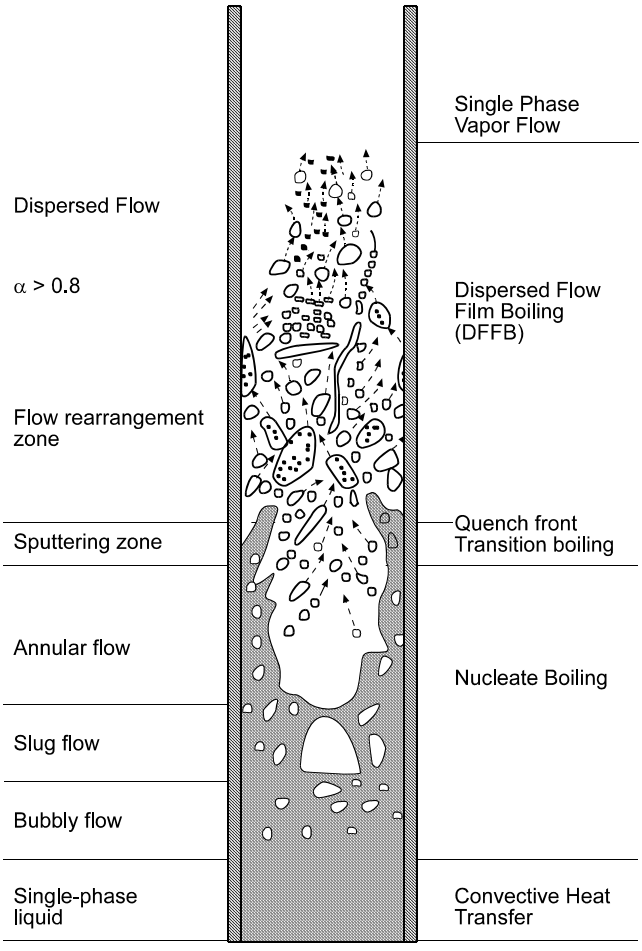

Figure 9: Flow regime description in a coolant channel after dry-out assuming very low re-wetting flow rate[9].

The physical principle which was used in the development of the present model to calculate the flow through the channel assumes that the hydrostatic pressure at the channel entrance must be equal to the static and the dynamic pressure drop created by the flow through the channel. This principle can be expressed by

$$\rho L_y g = \Delta P_{st} + \Delta P_f + \Delta P_a + \Delta P_{io}$$

Where:

ρ – coolant density

L_y – pool water level

g – gravitational constant

ΔP_{st} – the hydrostatic pressure drop in the channel obtained by integrating the coolant density along the channel $g \int \rho(y)\,dy$

ΔP_f – frictional pressure drop in the channel

ΔP_a. – Pressure drop due to accelerating the fluid along the channel

ΔP_{io} – entrance and exit pressure drops

The above equation serves as the basis for the momentum equation. In addition, the mass and energy balance equations were solved for the fuel channel to calculate all the system relevant state variables.

The computational fuel channel model developed for this study is presented schematically in Fig. 10. It is a two-dimensional model having an arbitrary number of nodes in the axial direction and three nodes in the radial direction, namely the fuel, the side plate and the water in the coolant channel. The model describes in detail the axial and radial heat conduction in the fuel, and from the fuel to the side plate and to the bottom grid plate and pool water, and convective heat transfer to the coolant flowing in the fuel channel. This model was included in the DSNP[1] (Dynamic Simulator for Nuclear Power-plants) library, which also includes many power plant components, material properties, heat-transfer and flow correlations[6,7] to be used with the simulation model. Full details of the mathematical model are subject to a detailed report[10]. Here only the principles are presented.

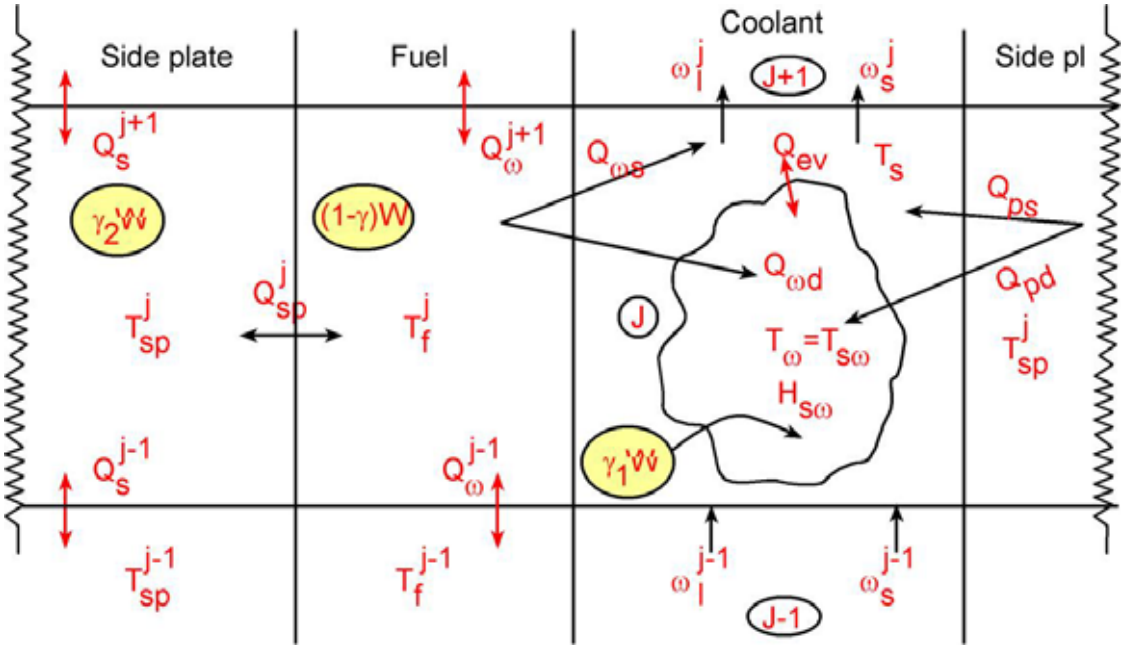

Figure 10: Schematic description of a MTR type fuel channel model.

Where:
T – Temperature
H - Enthalpy
w – Flow rate (Erroneously w is shown in the figure as ω)
w_ℓ – Water flow rate
w_d – Flow entering the channel to maintain an equilibrium pressure drop (ω_d in the figure)
w_{ev} – Evaporation rate from water slugs or drops
W – Decay heat power generated in the fuel
Q_w^{j+1} – Heat transfer between the j-th and the j+1-th axial region
Q_w^{j-1} – Heat transfer between the j-th and the j-1-th axial region
Q_{ws} – Heat convection between the fuel plate and the steam
Q_{wd} – Heat convection between the fuel plate and the water slugs/drops
Q_{sd} – Heat convection between water slugs/drops and the steam
Q_{pd} – Heat convection between side plate and water slugs/drops
Q_{ps} – Heat convection between side plate and the steam
γ_1 –Part of the decay heat released in water - γ radiation
γ_2 –Part of the decay heat released in the side plates
$\gamma = 1 - \gamma_1 - \gamma_2$ – Part of the decay heat released in the fuel
Indices
f – fuel
s – steam
sw – saturated water
ℓ - water
w – wall
sp – side plate
j-1, j, j+1, node indexing

The basic heat balance is presented by the two equations below (with the symbols given in Fig. 10)

$$\gamma W_f - Q_w^{j+1} - Q_w^{j-1} - Q_{sp}^j = Q_{wd} + Q_{ws}$$
$$\gamma_2 W_f - Q_s^{j+1} - Q_s^{j-1} + Q_{sp}^j = Q_{pd} + Q_{ps}$$

In the present model all radiative heat transfer between the wall and steam/droplets and between adjacent fuel plates is neglected. The water slugs and droplets drifting along the channel are assumed to be at saturation temperature, while the steam is being super-heated. The transfer between the steam and droplets results in additional evaporation along the channel.

Part of the heat generated in the fuel does not reach the coolant in the channels, rather it is conducted to the bottom and top end of the fuel rods. At the bottom it is conducted to the massive aluminium grid plate, and from there to the pool of water. At the top of the channel the heat is conducted to the aluminium part of the fuel rod entrance and then transmitted to the steam escaping from the channel. All these phenomena are included in the present model[10].

5 CONCLUSIONS

A two-dimensional model for a MTR type fuel rod was successfully developed and incorporated into the DSNP simulation package. From the simulation of the partial LOCA event in the MTR fuelled IAEA generic 10MW reactor, it can be concluded that the temperatures during the accident remains significantly below the Al softening temperature and no damage to the core is expected. These results are supported by the experiment performed in Livermore [5].

REFERENCES

[1] D. Saphier, *The DSNP User's Manual, Dynamic Simulator for Nuclear Power-plants*, RASG-115-85, Soreq Nuclear Research Centre, Yavne (1991)

[2] W. Zhang, T. Hibiki, K. Mishima, *Correlation, for Flow Boiling Heat Transfer at Low Liquid Reynolds Number in Small Diameter Channels*. Transactions of ASME, 127 (2005) 1214-1221

[3] W. M. Roshenow, J.P. Hartnett, Y.I. Cho, *Handbook of Heat Transfer*, Third Edition, McGraw Hill, (1998).

[4] IAEA: *Research Reactor Core Conversion Guidebook*, IAEA-TECDOC-643 (1992).

[5] UCRL, *Safety Analysis Report for Livermore Pool Type Reactor,* UCRL 51423, Chap 15 – Accident Analysis. (1974-revised)

[6] I. Silverman, *An external Material Properties, Heat Transfer and Flow Correlations Library for DSNP*, Soreq Nuclear Research Centre, Internal Report # 2738, RASG-214-97 (1997)

[7] D. Saphier, *The DSNP Material Properties Library*, RASG-117-85 Rev 4.3, Soreq Nuclear research center, (1991).

[8] J. Dreier, H. Winkler, *Results of the Mock-up Experiment on Partial LOCA.* The international meeting on reduced enrichment for research and test reactors, Tokai, JAERI, October (1983).

[9] L.E. Hochreiter, et. Al. Dispersed Flow Heat Transfer Under Re-flood Conditions in a 49 Rod Bundle, NUREG / C R-6671; PSU ME/NE – NRC-04-98-041 Report 1, (2000).

[10] D. Saphier, M. Betane, *A Computational Model for the Behavior of a Fuel Rod in the IAEA Generic Research Reactor for the DSNP Simulation System.* Soreq NRC, Yavne, internal report (in Hebrew), RASG—271-05, (2005).

European Nuclear Society

Rue Belliard 65
1040 Brussels
Belgium
Telephone +32 2 505 30 54
Fax + 32 2 502 39 02

topsafe2008@euronuclear.org

www.euronuclear.org